# A dominant-negative avirulence effector of the barley powdery mildew fungus provides mechanistic insight to barley MLA immune receptor activation

Emma E Crean[$,1], Merle Bilstein-Schloemer[$,1], Takaki Maekawa[1,2,3], Paul Schulze-Lefert[2,3], Isabel ML Saur[1,3]

[$] equal contribution

[1] Institute for Plant Sciences University of Cologne, Cologne, D-50674, Germany

[2] Department for Plant Microbe Interactions, Max-Planck Institute for Plant Breeding Research, 50829 Cologne, Germany

[3] Cluster of Excellence on Plant Sciences (CEPLAS)

Author for correspondence: isabel.saur@uni-koeln.de

## Abstract

Nucleotide-binding leucine-rich repeat receptors (NLRs) recognize pathogen effectors to mediate plant disease resistance, which is often accompanied by a localized host cell death response. Effectors can escape NLR recognition through various polymorphisms, allowing the pathogen to proliferate on previously resistant host plants. The powdery mildew effector $AVR_{A13}$-1 is recognized by the barley NLR MLA13 and activates host cell death. We demonstrate here that a virulent form of $AVR_{A13}$, called $AVR_{A13}$-V2, escapes MLA13 recognition by substituting a serine for a leucine residue at the C-terminus. Counterintuitively, this substitution in $AVR_{A13}$-V2 resulted in an enhanced MLA13 association and prevented the detection of $AVR_{A13}$-1 by MLA13. Therefore, $AVR_{A13}$-V2 is a dominant-negative form of $AVR_{A13}$ and has likely contributed to the breakdown of *Mla13* resistance. Despite this dominant-negative activity, $AVR_{A13}$-V2 failed to suppress host cell death mediated by the MLA13 auto-active "MHD" variant. Neither $AVR_{A13}$-1 nor $AVR_{A13}$-V2 interacted with the MLA13 auto-active variant, implying that the binding moiety in MLA13 that mediates association with $AVR_{A13}$-1 is altered after receptor activation. We also show that mutations in the MLA13 coiled-coil signalling domain, which were thought to impair $Ca^{2+}$-channel activity and NLR function, instead resulted in MLA13 auto-active cell death. The data constitute an important step to define intermediate receptor conformations during NLR activation.



## Key words

Mildew locus A, MLA, *Blumeria graminis*, fungal effector, NLR, resistance, powdery mildew, barley, cell death


## Short title:

A fungal avirulence effector dominantly inhibits the barley MLA immune receptor

## Introduction

During infection of their host, pathogens secrete numerous molecules that act either extracellularly or inside host cells. Some of these molecules act as virulence factors (so-called effectors) to manipulate the host's physiology in favour of the pathogen. Disease resistance of a plant against a pathogen is often mediated by resistance genes encoding nucleotide-binding leucine-rich repeat receptors (NLRs) (Maekawa *et al.*, 2011*b*; Jones *et al.*, 2016). NLRs recognize effectors by direct binding or by indirectly detecting effector-mediated alterations of host targets (guardees) or their mimics (decoys) (Cesari, 2018). Effector-mediated NLR activation is often linked to localized host cell death (Dodds and Rathjen, 2010; Saur and Hückelhoven, 2021; Maekawa *et al.*, 2022) and recognized effectors are called avirulence (AVR) effectors. Diversification of genes encoding AVRs can lead to loss of recognition by the respective NLR, resulting in pathogen virulence and breakdown of disease resistance (Märkle *et al.*, 2022). In case of direct AVR recognition, the NLR can usually no longer bind the diversified effector proteins of virulent pathogen isolates (Saur *et al.*, 2021).

NLRs are modular multidomain proteins with a central NB (nucleotide-binding) domain and C-terminal leucine-rich repeats (LRRs). At the N-terminus, most NLRs encode either a Toll/Interleukin-1 receptor-like (TIR) or a coiled-coil (CC) domain, classifying the majority of NLRs into either TIR-type NLRs (TNLs) or CC-type NLRs (CNLs) (Shao *et al.*, 2016). A subgroup of CNLs (also called RPW8-like NLRs or RNLs) are the helper NLRs NRG1 (N REQUIREMENT GENE 1) and ADR1 (ACTIVATED DISEASE RESISTANCE GENE 1) that are genetically required for TNL-mediated disease resistance (Saile *et al.*, 2020). The N-terminal CC and TIR domains mediate NLR signal emission upon NLR activation (Swiderski *et al.*, 2009; Bernoux *et al.*, 2011; Collier *et al.*, 2011; Maekawa *et al.*, 2011*a*; Williams *et al.*, 2014). In the absence of matching pathogen effectors, CC and TIR domains are locked in inactive conformations and this auto-inhibition is mediated by inter-domain interactions between the N-terminal domains with the NB and LRR domains (Burdett *et al.*, 2019; Saur *et al.*, 2021; Tamborski *et al.*, 2022). Although structural information on intermediate forms between inactive and active signalling NLRs is limited to the structure of the *Arabidopsis thaliana* CNL ZAR1 (HOPZ-ACTIVATED RESISTANCE 1) (Wang *et al.*, 2019*b*),

NLR activation is thought to be a multistep process (Förderer *et al.*, 2022*b*). The first activation step is ligand binding, which induces a steric clash between the LRR and the NB domain. The resulting open conformation of the NB domain then allows exchange of ADP (inactive) to ATP (active), which in turn induces allosteric changes to release the conformational auto-inhibition of the CC or TIR domains. This induces NLR oligomerization and these NLR oligomers are referred to as resistosomes (Förderer *et al.*, 2022*b*). Certain amino acid replacements within the conserved MHD motif of the NB domain mimic ATP binding and thus result in an active NLR conformation (Dinesh-Kumar and Baker, 2000; Bendahmane *et al.*, 2002; Paulmurugan *et al.*, 2002; Howles *et al.*, 2005; Gao *et al.*, 2011; Bai *et al.*, 2012; Ntoukakis *et al.*, 2013, 2014; Roberts *et al.*, 2013; Nishimura *et al.*, 2017). The N-terminal portion of the LRR domain in CNLs also contributes to receptor auto-regulation through interactions with CC and NB domains and amino acid exchanges at these sites can affect NLR auto-activity (Rairdan and Moffett, 2006; Slootweg *et al.*, 2013; Burdett *et al.*, 2019; Förderer *et al.*, 2022*a*; Tamborski *et al.*, 2022). For receptor activation *via* direct effector recognition, amino acids in the LRR can have additional functions as effector contact sites and can define the specificity of effector recognition (Jia *et al.*, 2000; Shen *et al.*, 2003; Dodds *et al.*, 2006; Bauer *et al.*, 2021; Tamborski *et al.*, 2022; Förderer *et al.*, 2022*b*). Upon direct effector recognition by the LRR or other integrated domains, effector binding correlates directly with NLR signal activation and studies on the *Magnaporthe oryzae* effectors AvrPik and AVR-Pia and the rice NLRs Pik and RGA5, respectively, argue for an affinity threshold between receptor and effector for activation of NLR immune signalling and pathogen resistance (Ortiz *et al.*, 2017; de la Concepcion *et al.*, 2018).

While the mechanisms underlying the restriction of pathogen growth by resistosomes is not fully elucidated, recent cryo-EM structures of multiple resistosomes (Wang *et al.*, 2019*a*,*b*; Ma *et al.*, 2020; Martin *et al.*, 2020; Förderer *et al.*, 2022*a*) revealed fundamental differences in immune signalling initiated by TNLs and CNLs: the pentameric resistosomes of *A. thaliana* ZAR1 CNL and wheat Sr35 CNL have calcium ion-permeable non-selective cation channel activity (Bi *et al.*, 2021; Förderer *et al.*, 2022*a*). The funnel-shaped ZAR1 cation channel is formed by the N-terminal CC domain α1-helix of the

ZAR1 resistosome (Wang *et al.*, 2019*a*,*b*). Substitutions of negatively charged amino acids to alanine in the inner lining of the funnel abolishes $Ca^{2+}$ channel and cell death activity and ZAR1-mediated resistance (Wang *et al.*, 2019*b*; Bi *et al.*, 2021). The α1-helix region of the wheat Sr35 resistosome is not well resolved in the cryo-EM structure and Sr35 α1-helix amino acid exchanges equivalent to those in ZAR1 do not affect AvrSr35-dependent Sr35 resistosome channel and cell death activity (Förderer *et al.*, 2022*a*; Zhao *et al.*, 2022), suggesting differences in $Ca^{2+}$ signalling functions between ZAR1 and Sr35 resistosomes. Effector binding to the TNLs RPP1 (RECOGNITION OF PERONOSPORA PARASITICA 1) and ROQ1 (RECOGNITION OF XopQ 1) from *A. thaliana* and *Nicotiana benthamiana*, respectively, induces the formation of homotetrameric complexes stimulating TIR enzyme activity. The resistosome TIR enzyme, but also TIR-only proteins, produce a variety of nucleotide-based second messenger molecules (Horsefield *et al.*, 2019; Wan *et al.*, 2019; Yu *et al.*, 2022; Huang *et al.*, 2022; Jia *et al.*, 2022), some of which serve as ligands to activate the EDS1 protein family plus the signalling/helper CNLs ADR1 or NRG1 (Lapin *et al.*, 2019; Huang *et al.*, 2022; Jia *et al.*, 2022). ADR1 and NRG1 can also function as calcium ion-permeable nonselective cation channels (Jacob *et al.*, 2021), and as such disruption of $Ca^{2+}$ homeostasis appears to be central in CNL and TNL resistosome signalling.

The polymorphic barley *Mildew locus A* (*Mla)* encodes allelic variants of CNLs (MLA NLRs), each conferring isolate-specific disease resistance to the barley powdery mildew fungus *Blumeria graminis* f. sp. *hordei* (*Bgh*) (Moseman and Schaller, 1960; Glawe, 2008; Seeholzer *et al.*, 2010; Maekawa *et al.*, 2019). Some barley MLA receptors and *Mla* homologs confer additional resistance to isolates of unrelated fungal pathogens (Periyannan *et al.*, 2013; Mago *et al.*, 2015; Chen *et al.*, 2017; Bettgenhaeuser *et al.*, 2021; Ortiz *et al.*, 2022; Brabham *et al.*, 2022). The *Bgh* effectors recognized by barley MLAs are known as $AVR_A$ effectors (Moseman and Schaller, 1960; Jorgensen, 1994) and diversified variants that have escaped *Mla* recognition are designated as $AVR_A$-V variants (Lu *et al.*, 2016). To date, full length structures of inactive or effector-activated MLAs are not available, but protein interaction assays suggest a direct interaction between at least some MLA NLRs and matching $AVR_A$ effectors (Saur *et al.*, 2019*a*). Most amino acids under positive selection of *Mla* resistance

specificities map to the predicted solvent-exposed sites of the LRR, suggesting that these serve as $AVR_A$ contact residues (Seeholzer *et al.*, 2010; Maekawa *et al.*, 2019), but interaction between effectors and MLA LRR domain deletion constructs could not be shown. Most of the known *Bgh* $AVR_A$ effectors are sequence-unrelated, but share a common fold reminiscent of ribonucleases lacking catalytic residues (Bauer *et al.*, 2021).

*Mla13* in barley confers resistance to most *Bgh* isolates representing a global pathogen population because these avirulent isolates express recognised $AVR_{A13}$-1/BLGH_02099 (Lu *et al.*, 2016; Saur *et al.*, 2019*a*). $AVR_{A13}$-1 is directly recognized by MLA13 and effector recognition drives MLA13-mediated cell death upon transient co-expression of *Mla13* and *$AVR_{a13}$*-1 in barley protoplasts and heterologous *N. benthamiana* leaves. *$AVR_{a13}$-1/BLGH_02099* is polymorphic in the *Mla13*-virulent *Bgh* isolates CC52 and B103 and the resulting gene products are named $AVR_{A13}$-V1 and $AVR_{A13}$-V2, respectively (Lu *et al.*, 2016). $AVR_{A13}$-V1 represents a truncated version of $AVR_{A13}$-1, and after transient gene overexpression *in planta*, the $AVR_{A13}$-V1 protein is unstable and often not detectable. Currently, it cannot be ruled out that the lack of $AVR_{A13}$-V1 recognition by MLA13 is solely due to $AVR_{A13}$-V1 protein instability (Saur *et al.*, 2019*a*). $AVR_{A13}$-V2 carries five C-terminal amino acids (VRATL) that correspond to eight unrelated amino acids in $AVR_{A13}$-1 (TCMVSSPE). Not in agreement with the virulent pathotype of *Bgh* isolate B103 on *Mla13* barley, interaction assays *in planta* and in yeast indicated a stable association between $AVR_{A13}$-V2 and MLA13 (Saur *et al.*, 2019*a*).

Because receptor-effector interaction is commonly linked to receptor activation, we aimed here to investigate the seeming paradox of MLA13 inactivity despite stable $AVR_{A13}$-V2 - MLA13 association By applying proximity-dependent protein labelling (BioID), yeast-2-hybrid (Y2H) interaction assays and structural prediction (Alphafold2) in combination with *in planta* expression of naturally occurring $AVR_{A13}$ effector variants and by generating deletion and hybrid constructs, we demonstrate that a single surface-exposed amino acid at the C-terminus of $AVR_{A13}$ effectors determines the association with and activation of MLA13. Our data also reveal that $AVR_{A13}$-V2 acts as dominant-negative effector on MLA13-mediated cell death. This proposes that breakdown of *Mla13*-mediated resistance can be

147 explained by *Bgh* isolates carrying dominant-negative $AVR_{A13}$-V2. We also demonstrate that amino acid
148 exchanges in the MLA13 NB and LRR domains compromise effector binding. In turn, amino acid
149 changes in the MLA13 CC domain predicted to disrupt cation channel activity, do not affect MLA13-
150 mediated cell death. Nevertheless, inhibition of $Ca^{2+}$ and other cation channels by $LaCl_3$ impaired
151 MLA13-mediated cell death of barley protoplasts. Collectively, these results provide insights and tools
152 for understanding the conformational changes NLRs undergo during effector-mediated NLR
153 resistosome activation.

154

155 ## Results

156 ### *The C-terminus of $AVR_{A13}$ effectors determines interaction with and activation of MLA13*

157 The C-terminally located polymorphisms between genes encoding avirulent $AVR_{A13}$-1 effector
158 (activates MLA13-specified cell death) and virulent $AVR_{A13}$-V1 or $AVR_{A13}$-V2 variants (unable to activate
159 MLA13 cell death; Fig. 1A) indicate a role of the $AVR_{A13}$-1 C-terminus in the interaction with and
160 activation of MLA13. Previously, no avirulence activity could be detected for $AVR_{A13}$-V1, but this could
161 be attributed to its protein instability upon transient expression *in planta* (Lu *et al.*, 2016; Saur *et al.*,
162 2019*a*). Here we aimed to stabilize $AVR_{A13}$-V1 protein by fusion with an epitope to retest the
163 association patterns of the $AVR_{A13}$ variants with MLA13 *in planta*. To this end, we fused the three
164 effector variants to a biotin ligase (BirA), and indeed this fusion allowed immunodetection of the
165 $AVR_{A13}$-V1 protein at levels comparable to the other two variants in *N. benthamiana* leaves (Fig. S1).
166 We also confirmed the functionality of the tagged proteins by demonstrating MLA13-specified cell
167 death induced by $AVR_{A13}$-1-BirA-4xMyc (Fig. S1). We detected biotinylated MLA13, but not MLA1 or
168 MLA7 protein, in samples expressing *Mla13-4Myc* together with *$AVR_{a13}$-1-BirA* or *$AVR_{a13}$-V2-BirA*, but
169 not *$AVR_{a13}$-V1-BirA* after biotin treatment followed by a streptavidin pull-down (Fig. S1B). Given that
170 $AVR_{A13}$-V1 lacks the 42 C-terminal amino acids of $AVR_{A13}$-1 (Fig. 1A), the data provides experimental

171 evidence that the C-terminal half of $AVR_{A13}$ is needed for the association and activation of MLA13
172 receptor.

173

174 Both, $AVR_{A13}$-1 and $AVR_{A13}$-V2 associate with MLA13, but only $AVR_{A13}$-1 activates MLA13-mediated cell
175 death (Saur *et al.*, 2019*a*) (Fig. S1). To delineate the $AVR_{A13}$-1 amino acids required for MLA13 cell death
176 activation, we generated a truncated $AVR_{A13}$-1 construct ($AVR_{A13}$-$1^{\Delta SPE}$) and four hybrid variants of
177 $AVR_{A13}$-1 and $AVR_{A13}$-V2, which differ from $AVR_{A13}$-$1^{\Delta SPE}$ by one, two, three and four C-terminal amino
178 acids, respectively (Fig. 1A). We then measured the ability of $AVR_{A13}$-$1^{\Delta SPE}$ and the hybrid variants to
179 induce MLA13-mediated cell death upon transient expression in *N. benthamiana* leaves (Fig. 1B and
180 1C). $AVR_{A13}$-$1^{\Delta SPE}$ was the only engineered construct that induced MLA13-specified cell death
181 comparable to $AVR_{A13}$-1 in these assays (Fig. 1B). Therefore, the three C-terminal amino acids are
182 dispensable for the avirulence activity of $AVR_{A13}$-1. The data demonstrates that the replacement of
183 serine to leucine at position 119 abrogated MLA13-mediated cell death in *N. benthamiana*, suggesting
184 that this serine in $AVR_{A13}$-1 and $AVR_{A13}$-$1^{\Delta SPE}$ is crucial for cell death activation (Fig. 1B).

185 MLA13 interacts more efficiently with $AVR_{A13}$-V2 than with $AVR_{A13}$-1, and this enhanced association
186 correlates with the inability to induce MLA13-mediated cell death (Saur *et al.*, 2019*a*). We therefore
187 tested the association of $AVR_{A13}$-$1^{\Delta SPE}$ and the $AVR_{A13}$-1/ $AVR_{A13}$-V2 hybrid variants with MLA13. Protein
188 stability of $AVR_{A13}$ hybrid variants varies *in planta,* which makes the assessment of quantitative
189 differences of the interactions difficult (Fig. 1C). We then used a Y2H assay drop out series to evaluate
190 putative quantitative differences, as in this system the corresponding prey and bait variants
191 accumulated to comparable levels. We fused *Mla* N-terminally to the *LexA* binding domain sequence
192 (*BD-Mla13*) and the $AVR_{a13}$ variant genes to the *B42* activation domain (*AD-*$AVR_{a13}$) and determined
193 yeast growth in the absence of leucine as a proxy for protein interaction. We found that yeasts co-
194 expressing *BD-Mla13* with the *AD-*$AVR_{a13}$*-1* and *AD-*$AVR_{a13}$*-*$1^{\Delta SPE}$ grew less in the dilution series than
195 yeasts carrying *AD-*$AVR_{a13}$*-V2* or any of the *AD-*$AVR_{a13}$ hybrid constructs (Fig. 1D). No growth was
196 detected when *BD-Mla13* was co-expressed with *AD-*$AVR_{a13}$*-V1* or when any $AVR_{a13}$ variant was co-

197 expressed with *BD-Mla1* (Fig. 1D and Fig. S2). The data imply that $L^{119}$ of $AVR_{A13}$-V2 (Fig. 1A) is
198 responsible for the enhanced interaction with MLA13. The corresponding residue in $AVR_{A13}$-1 is a
199 serine. We generated structural predictions of the $AVR_{A13}$ variants (lacking the respective signal
200 peptides (SP)) using AlphaFold2 ($pLDDT_{overall}$ = 89, $pLDDT_{L/S119}$ = >80) to determine if either of these
201 residues are surface exposed. Indeed both, $L^{119}$ of $AVR_{A13}$-V2 ΔSP and $S^{119}$ of $AVR_{A13}$-1 ΔSP appear to be
202 surface exposed in these structural models, suggesting that they are accessible for binding to MLA13
203 (Fig. 1F).

204

205 ***$AVR_{A13}$-V2 can act as dominant-negative effector on MLA13-mediated cell death***

206 The observed enhanced association between MLA13 and $AVR_{A13}$-V2 could affect *Mla13* disease
207 resistance and possibly the activity of other MLA NLRs with resistance specificity to *Bgh*. To test this,
208 we measured $AVR_A$-induced MLA-mediated cell death in the presence of $AVR_{A13}$-V2. Co-expression of
209 *Mla13-4xMyc* together with *$AVR_{a13}$-1-mYFP* (monomeric YFP) and an *empty vector* (*EV*) in
210 *N. benthamiana* leaves resulted in a cell death response within 50 to 72 hours post infiltration and this
211 response was not detectable when EV was exchanged for *$AVR_{a13}$-V2-mYFP* (Fig. 2A). We also tested
212 whether *$AVR_{a13}$-V2-4xMyc* affects cell death mediated by *Mla1-3xHA* and *$AVR_{a1}$-mYFP* or *Mla7-3xHA*
213 and *$AVR_{a7}$-2-mYFP* after transient expression of the constructs in *N. benthamiana*. We assessed the
214 severity of cell death on a scale from 0 to 3 and found that $AVR_{A13}$-1 and MLA13-mediated cell death
215 was abrogated by the co-expression of $AVR_{A13}$-V2. By contrast, cell death in samples expressing *$AVR_{a13}$-*
216 *V2* alongside *Mla1* and *$AVR_{a1}$* or *Mla7* and *$AVR_{a7}$-2* were comparable to those in which *$AVR_{a13}$-V2* was
217 replaced by *EV* or *$AVR_{a13}$-V1* (Fig. 2B). The specific inhibitory effect of *$AVR_{a13}$-V2* on the MLA13 receptor
218 (Fig. 2B) is not due to interference with MLA13 or $AVR_{A13}$-1 protein stability, as both proteins were
219 detectable at similar levels in samples with EV or unstable $AVR_{A13}$-V1 as in samples co-expressing
220 *$AVR_{a13}$-V2* (Fig. 2C). Our data suggest that $AVR_{A13}$-V2 has a dominant-negative effect on cell death
221 activity specifically mediated by MLA13.

### *Amino acid exchanges in the nucleotide-binding site of MLA13 compromise $AVR_{A13}$ effector binding*

Previous reports on flax TNL L6 suggest an equilibrium between inactive and active NLR conformations in the absence of pathogen effectors, but that binding of the matching effector stabilizes the active NLR conformation (Bernoux *et al.*, 2016). We therefore hypothesized that avirulent $AVR_{A13}$-1 stabilizes the active ATP-bound oligomeric conformation of MLA13. Given that $AVR_{A13}$-V2 can inhibit MLA13-mediated cell death in the co-expression assays (Fig. 2), we hypothesized that $AVR_{A13}$-V2 binds and stabilizes the inactive MLA13 receptor. To test this hypothesis, we applied the aforementioned Y2H approach to examine the interaction between naturally occurring $AVR_{A13}$ variants and MLA13 variants carrying mutations in the NB domain that render the receptor inactive (P-loop mutants that cannot bind ADP or ATP at the NB domain) or auto-active (MHD mutant mimicking ATP binding at the NB domain). We first confirmed that the MLA13 P-loop mutant ($MLA13^{K207R}$) is unable to induce cell death upon co-expression with $AVR_{A13}$-1 (Fig. S3A) and that $MLA13^{D502V}$ (MHD mutant) induces cell death in the absence of the matching effector (Fig. S3B), before testing their ability to bind $AVR_{A13}$ variants in yeast. In the Y2H assay, yeast expressing BD-MLA13 together with AD-$AVR_{A13}$-1 or AD- $AVR_{A13}$-V2, but not AD-$AVR_{A13}$-V1 fusion protein, grew as expected. Interestingly, none of the yeast samples co-expressing BD-$MLA13^{D502V}$ or BD-$MLA13^{K207R}$ together with any $AVR_{A13}$ variants grew in the absence of leucine although all proteins were stably detectable by western blot (Fig. 3A and 3B). We observed similar results for the *Mla* homolog *Sr50*, although we detected growth of yeast expressing AD-AvrSr50 with the MHD variant $Sr50^{D498V}$ fused N-terminally to the B42 BD (Fig. S3). However, the latter interaction was consistently weaker when compared to samples co-transformed with BD-Sr50 wild-type (WT) and AD-AvrSr50. When AD-AvrSr50 was replaced by AD-$AvrSr50_{QCMJC}$, a variant lacking avirulence activity, no interaction was detected, which was not due to differences in protein levels between the tested effector variants (Fig. S3C and S3D).

$AVR_{A13}$-V2 binds specifically and strongly to wild-type MLA13 and can inhibit MLA13-specified cell death signalling, suggesting a direct link between effector binding and cell death inhibition for this

association. However, $AVR_{A13}$-V2 cannot bind auto-active $MLA13^{D502V}$ in the Y2H assay (Fig. 3A) and we therefore speculate that it cannot inhibit $MLA13^{D502V}$-mediated cell death. Indeed, co-overexpression of *$AVR_{a13}$-V2* or *$AVR_{A13}$-V1* had no effect on the average cell death score of $MLA13^{D502V}$-induced cell death observed as early as two days post Agroinfiltration (dpi) of the respective constructs in *N. benthamiana* leaves (Fig. 3C). Four to five days after infiltration of *N. benthamiana* leaves with Agrobacteria carrying *35S:Mla13* at $OD_{600}$=1, we also detected effector-independent cell death mediated by wild-type MLA13 (MLA13 auto-activity). This average cell death score of 2 was significantly impaired in samples co-overexpressing *$AVR_{a13}$-V2* (average cell death score = 0.5) but not *$AVR_{a13}$-V1* (average cell death score = 1.9). Compared with *EV* or unstable *$AVR_{a13}$-V1*, co-expression of *$AVR_{a13}$-V2* had no effect on the protein levels of any of the MLA13 variants used (Fig. 3D). Of note, cell death mediated by overexpression of the MLA13 CC domain ($MLA13^{CC}$, amino acid (aa) 1-160) was not affected by $AVR_{A13}$-V2 (Fig. S3E and S3F).

## *Different affinities between MLA13 mutant variants and $AVR_{A13}$ effectors*

The lack of $AVR_{A13}$ interaction with both inactive and active CNL MLA13 mutant variants was unexpected, as it contrasts with previous reports on flax TNL L6 and its matching effector AvrL567 (Bernoux *et al.*, 2016). We therefore investigated whether this lack of effector-receptor association could be generalized to other putatively inactive or auto-active MLA13 variants (Fig. 4A). In addition to the $MLA13^{D502V}$ and $MLA13^{K207A}$ variants (Fig. 3), we chose the MHD mutant variant H501G, whose auto-activity in MLA10 appears to be less pronounced than that of D502V (Bai *et al.*, 2012). Receptor auto-activity was also previously reported for the F99E (mutation in the CC domain) variant of MLA10 (Bai *et al.*, 2012). We also included the D284A mutant (mutation in the walker A motif of the NB site, Fig. 4A) because the corresponding variant in the *A. thaliana* CNL RPM1 (RESISTANCE TO P. SYRINGAE PV MACULICOLA 1) leads to RPM1 auto-activity (Gao *et al.*, 2011). By substituting negatively charged residues in the first α-helix of MLA13 to alanine ($MLA13^{D2A\_E17A}$), we aimed to generate an MLA13 resistosome that is structurally intact but impaired in immune signalling via $Ca^{2+}$ influx (Wang *et al.*, 2019*a*,*b*; Bi *et al.*, 2021). This hypothesis is based on the observation that the replacement of negatively

charged amino acids in the α1-helix of ZAR1 abrogates $Ca^{2+}$ influx and impairs cell death activity and ZAR1 disease resistance, but not formation and membrane association of the ZAR1 resistosome (Wang *et al.*, 2019*a*,*b*; Bi *et al.*, 2021). The S902F_F935I substitutions affect residues in the 14th and 15th LRRs of MLA13 (Fig. 4A) and the corresponding receptor is not expected to detect $AVR_{A13}$-1 as it is encoded by the barley line SxGP DH-47 (cross of cultivars SusPtrit and Golden Promise), which is fully susceptible to *Bgh* isolates carrying avirulent *$AVR_{a13}$* (Bettgenhaeuser *et al.*, 2021).

We first tested our assumption that the MLA13 mutants exhibit altered cell death activities (inactive/auto-active) compared to wild-type. We expressed the corresponding gene constructs in *N. benthamiana* leaves and qualitatively determined cell death in the presence and absence of $AVR_{A13}$-1. As reported for other MLA variants (Bai *et al.*, 2012), $MLA13^{H501G}$ and $MLA13^{F99E}$ showed effector-independent cell death activity in this assay. In contrast, the Walker A-motif mutant $MLA13^{D284A}$ and SusPtritis $MLA13^{S902F\_F935I}$ receptor variants are unable to trigger host cell death when expressed together with *$AVR_{a13}$-1*. However, expression of $MLA13^{D2A\_E17A}$, which is thought to be impaired in $Ca^{2+}$ and cell death signalling (Bi *et al.*, 2021), resulted in effector-independent cell death in *N. benthamiana* leaves within 2 dpi (Fig. 4B). All MLA13 variants are detectable as fusion proteins after transient expression in *N. benthamiana* (Fig. 4C).

We next determined the ability of $AVR_{A13}$-V2 to bind $MLA13^{H501G}$, $MLA13^{F99E}$, $MLA13^{D284A}$, $MLA13^{D2A\_E17A}$ and $MLA13^{S902F\_F935I}$ in a Y2H assay. Again, $MLA13^{D502V}$ and $MLA13^{K207R}$ variants served as negative controls. Yeast samples expressing *AD_$AVR_{a13}$-V2* together with wild-type *BD-Mla13* grew to a dilution of OD600 = 0.001 and to a dilution of OD600 = 0.01 when wild-type MLA13 was replaced with $MLA13^{D2A\_E17A}$ or $MLA13^{F99E}$. When wild-type MLA13 was replaced by $MLA13^{D284A}$, $MLA13^{K207R}$ o $MLA13^{S902F\_F935I}$ showed growth in the absence of leucine (Fig. 4D) although these MLA13 variants are stably expressed in yeast (Fig. 4E). The MLA F99 residue is not conserved in other CNLs and therefore, the currently available CNL resistosome structures of ZAR1 and Sr35 cannot give functional insight to the role of this residue. However, the ZAR1 resistosome structures postulate that upon ligand binding, the release of the α1-helix in CNLs is an important conformational change that occurs immediately

before resistosome formation (Wang *et al.*, 2019*a*,*b*). We thus speculate that the auto-activity of MLA13$^{D2A_E17A}$ is a result of mutation-induced α1-helix release. If this is the case, then this auto-activity cannot be inhibited by the dominant-negative $AVR_{A13}$-V2 ligand. When compared to EV, co-expression of *$AVR_{a13}$-V2-mYFP* with MLA13$^{D2A_E17A}$ in *N. benthamiana* leaves had indeed no impact on the average cell death score, whereas auto-activity of wild-type MLA13 was again inhibited by co-expression of *$AVR_{a13}$-V2-mYFP* (Fig. 4F).

## *Activity of cation channels is required for MLA13 cell death*

In ZAR1, the negatively charged residues on the inner lining of the ZAR1 resistosome funnel are required for $Ca^{2+}$ channel activity, and substitutions of these amino acids impaired ZAR1 signalling (Bai *et al.*, 2012; Wang *et al.*, 2019*b*). By contrast, such substitutions in Sr35 had no effect on cell death or channel activity (Förderer et al., 2022a), and the same appears to be true for MLA13 D2A_E17A (Fig. 4B). The data suggest that MLA13 does not require the negatively charged amino acids of the α1-helix in the CC domain for cell death signalling. We thus aimed to determine whether $Ca^{2+}$ channel activity is needed for MLA13-mediated cell death in barley by applying the potent cation channel inhibitor $LaCl_3$. Toward this end, we expressed a luciferase (LUC) reporter together with *$AVR_{a13}$-1* in barley mesophyll protoplasts, prepared from the *Mla13*-containing near-isogenic backcross line Manchuria (CI 16155), and measured LUC activity as an indicator of protoplast viability. Protoplasts from the cultivar Manchuria (CI 2330), which lack *Mla13*, served as control. With increasing $LaCl_3$ concentration, we observed a reduction in LUC activity by up to 50% of CI 2330 protoplasts (20 µM $LaCl_3$), suggesting a detrimental impact of $LaCl_3$ treatment on protoplast viability independent of *Mla13* or a reduction in LUC activity independent of cell death. Nonetheless, in the absence of $LaCl_3$, LUC activity is on average more than 70% lower in *Mla13* protoplasts transfected with the *$AVR_{a13}$-1* construct than in protoplasts that do not express *Mla13* (Fig. 5A). This difference in LUC activity between the two samples diminishes with increasing $LaCl_3$ concentration and is no longer significant in samples treated with 10 µM $LaCl_3$. Although LUC activity decreases with increasing $LaCl_3$ concentrations, $LaCL_3$ treatment does not affect

$AVR_{A13}$-1 protein stability in protoplasts of the cultivar Manchuria (Fig. 5B). Although we cannot exclude that $LaCl_3$ treatment affects *Mla13* expression in barley line CI 16155, our data show that blocking the function of cation channels by $LaCl_3$ compromises MLA13-mediated cell death in barley leaf protoplasts.

## Discussion

Functional studies of effector recognition by NLRs are not only important for a better understanding of plant disease resistance but also for dissecting the mechanisms pathogens employ to overcome NLR-mediated resistance. To address both aspects, we studied MLA13-mediated recognition of the barley powdery mildew $AVRa_{A13}$ effector family with a particular focus on $AVR_{A13}$-V2, which originated from a *Bgh* isolate that has overcome *Mla13* resistance.

### Mutations in the NB site of MLA13 abrogate association with its matching effector

The residues of the MLA LRR domains, which are under purifying selection, are thought to serve as effector contact residues (Seeholzer *et al.*, 2010; Maekawa *et al.*, 2019). Residues $S^{902}$ and $P^{935}$ in the $14^{th}$ and $15^{th}$ LRRs of MLA13 are exchanged for other amino acids in MLA13 encoded by a cultivar that has lost *Mla13* resistance function (Bettgenhaeuser et al., 2021), and we showed here that the residues are indeed required for effector binding and activation of MLA13. Importantly, however, our data show that not only the contact residues in the NLR LRR domain mediate receptor-effector association, but that an intact, ADP-bound receptor conformation is required for efficient effector-receptor association in yeast. Disruption of this intact conformation by mutations in the NB site of MLA13, which result in the so-called 'MHD' (mimicking ATP binding) and 'P-loop' (no binding of ADP/ATP) receptor versions (Fig. S4) fully abrogated interaction with the matching $AVR_{A13}$ effector variants in Y2H assay, probably because of spatial hindrance. One possible explanation for this hindrance is that residues of the MLA13 NB domain are engaged in the formation of an effector-accessible conformation of the MLA LRR domain, i.e. a site of effector entry (Förderer *et al.*, 2022*b*) only provided by ADP-bound MLA13 (Fig.

S4). At this effector entry site of ADP-bound MLA13, the MLA13 NB domain may transiently contact the $AVR_{A13}$ ligand and this contact may be required for the the steric clash that dislocates the NB domain for exchange of ADP to ATP. In fact, one intermediate state structure of the ADP-bound ZAR1 monomer bound to the activating PBL2 ligand (PDB 6j5v) implies contact between the ZAR1 NB domain and the PBL2 ligand ultimately before the steric clash that allows effector-mediated ZAR1 resistosome formation, although association between the contact-forming residues cannot be detected in the active, ATP-bound ZAR1 resistosome (Wang *et al.*, 2019*b*). An alternative hypothesis of our findings is a transient association between $AVR_{A13}$ and MLA13, implying that conformational changes of MLA13 to the active oligomeric ATP-bound state lead to dislodging of $AVR_{A13}$ effectors from the resistosome complex. However, this model is in contrast with the observation of all active NLR resistosome structures available to date, where each NLR monomer stably binds one activating ligand. The autoactive wheat CNL $Sr50^{MHD}$ mutant was also impaired in AvrSr50 association when compared to wild-type Sr50 (Fig. S3), but our data contrast with the example of enhanced association between the flax TNL L6 MHD version and its matching effector (Bernoux *et al.*, 2016). We therefore suggest different requirements for NB domains at the site of effector entry in CNLs and TNLs or for individual NLRs in general. However, we cannot entirely exclude that this difference may be due to the initiation of yeast cell death upon expression of $CNL^{MHD}$, whereas $TNL^{MHD}$ variants cannot induce cell death in yeast. However, the $MLA13^{MHD}$ and $Sr50^{MHD}$ protein levels are as stable as those of wild-type receptors and yeast growth in the presence of leucine is similar between yeasts expressing wild-type receptors and the MHD variants (Fig. 3B and Fig. S3D).

We and others have previously attempted to detect interaction between CNLs and their matching effector *in planta* by using NLR P-loop mutants to prevent NLR-mediated cell death. Blocking TNL ROQ1-mediated cell death signalling in *eds1* knockout lines in *N. benthamiana* was important for purification of the tetrameric ROQ1-effector resistosome (Martin *et al.*, 2020). Our data showing that MLA13 P-loop variants have lost the ability to bind matching effectors might explain why previous attempts to detect effector – receptor interaction using P-loop CNL mutants were unsuccessful.

**Amino acid exchanges in the MLA13 α1-helix deregulate auto-inhibition but not $Ca^{2+}$ - dependent MLA13 cell death function.**

Negatively charged residues in the α1-helix of NLR CC domains are thought to be required for $Ca^{2+}$ channel activity of CNL resistosomes (Förderer *et al.*, 2022*b*). This was inferred from the observation that replacement of these residues with alanine abrogated ZAR1 $Ca^{2+}$ channel activity and ZAR1-mediated resistance. We observed that the negatively charged residues $MLA13^{D2}$ and $MLA13^{E17}$ in the α1-helix are not required for MLA13-mediated cell death and that these amino acid exchanges instead lead to effector-independent cell death in *N. benthamiana*. We speculate that in the absence of a matching effector, these negatively-charged amino acids in MLA13 are required for burying the α1-helix and that this auto-repression malfunctions in $MLA13^{D2A\_E17A}$, i.e. the α1-helix is exposed and available for oligomerization (Fig. S4). However, our data cannot clarify whether the hypothetical auto-active α1-helix conformation of $MLA13^{D2A\_E17A}$ allows the exchange of ADP to ATP or whether an ADP-bound NB domain is even capable of forming a functional oligomer (Fig. S4).

The cell death autoactivity of $MLA13^{D2A\_E17A}$ contrasts with similar ZAR1 mutants, which abolish cell death, but the data is comparable to results reported for other CNLs, including wheat Sr35 (Adachi *et al.*, 2019; Förderer *et al.*, 2022*a*). Despite these differences, we demonstrate that MLA13-dependent and $AVR_{A13}$-triggered cell death activity in barley protoplasts is impaired in the presence of the cation channel inhibitor $LaCl_3$, suggesting that cation transport across plant cell membranes by a putative MLA13 channel and/or other cation channels is also an important biochemical activity of the deduced MLA13 resistosome. Although the exact mechanism for cation transport in the putative MLA13 resistosome remains to be determined, our data align with reports on other CNLs that confer calcium channel-dependent cell death (Grant *et al.*, 2000; Förderer *et al.*, 2022*a*) and underline that perturbation of $Ca^{2+}$ homeostasis is a fundamental component of both, TNL- and CNL-mediated cell death in plants (Jubic *et al.*, 2019; Saur *et al.*, 2021; Jacob *et al.*, 2021; Förderer *et al.*, 2022*a*).

**A single effector residue can disrupt NLR activation**

As LRR domains have the potential to bind a variety of proteinaceous ligands, engineering the LRR domains of NLRs to bind pathogen effectors that are not recognized by the natural immune system appears to be an attractive strategy for controlling plant diseases. Our data demonstrate that ligand binding *per se* is not sufficient for NLR activation and that a single surface-exposed residue, $L^{119}$ in full-length $AVR_{A13}$-V2, can abrogate NLR activation despite enhanced interaction. This dominant-acting interaction may directly allow $AVR_{A13}$-V2 to outcompete all $AVR_{A13}$-1 effectors for association with MLA13 and subsequent receptor activation. Alternatively, $AVR_{A13}$-V2 sequestration of some MLA13 monomers might be sufficient to disrupt putative MLA13 resistosome formation if a threshold of ligand-activated CNLs must be available for pentameric CNL resistosomes to be formed (Förderer *et al.*, 2022*b*). The possibility that $AVR_{A13}$-V2 sequesters $AVR_{A13}$-1 from activation of MLA13 appears less likely because $AVR_{A13}$-V2 can also inhibit MLA13 auto-activity (Fig. 2). The contact residues responsible for the activation of MLA13 by $AVR_{A13}$ are likely unique, despite the overall structural similarity of $AVR_A$ effectors and allelic, highly sequence similar MLA receptors (Seeholzer *et al.*, 2010; Bauer *et al.*, 2021). This appears to be also true for the residues of $AVR_{A13}$-V2 (including $L^{119}$) that mediate MLA13 interaction, as neither the enhanced interaction, nor the dominant-negative effect of $AVR_{A13}$-V2 was detected when MLA13 was replaced by the highly sequence-similar MLA1 or MLA7 NLRs. The overall high sequence and predicted structural identity between $AVR_{A13}$-1 and $AVR_{A13}$-V2, as well as the identification of a single residue, $L^{119}$ of $AVR_{A13}$-V2, as the main driver of enhanced MLA13 interaction, suggest that the binding surfaces to the MLA13 receptor overlap. However, our data implies that $AVR_{A13}$-V2 locks MLA13 into an inactive, effector-bound state by preventing the receptor from transitioning to one of the conformational changes downstream of effector binding (Fig. S5). $AVR_{A13}$-V2 cannot inhibit cell death signalling of MLA13 constitutive-gain of function mutants with amino acid replacements in the CC domain despite interaction with $MLA13^{D2A\_E17A}$ (Fig. 4D). We therefore suggest that the inhibitory function of $AVR_{A13}$-V2, mediated by $L^{199}$, affects conformational changes that take place before the release of the MLA13 α1-helix; i.e. $AVR_{A13}$-V2 binding to MLA13 either fails to induce an inter-domain steric clash in the receptor or blocks the transition to the steric clash-mediated open conformation, which allows exchange of ADP to ATP in the NB site of MLA13 (Fig. S5). Alternatively,

AVR$_{A13}$-V2 binding to MLA13 induces a steric clash, but AVR$_{A13}$-V2 association inhibits the release of the α1-helix from autorepression. As MLA13 MHD mutants are generally inaccessible to effector binding in Y2H assay (including binding to avirulent AVR$_{A13}$-1), our data cannot clarify whether the loss of inhibitory function of AVR$_{A13}$-V2 on MLA13 cell death takes place before or after ADP exchange to ATP in wild-type MLA13. Collectively, we demonstrate that the stable interaction between AVR$_{A13}$-V2 and inactive MLA13 has the potential to define distinct conformations of intermediate states of CNL receptors. This knowledge is currently largely elusive for both animal and plant NLRs. Understanding such conformations will help ensure that future synthetic NLRs do not become locked into intermediate non-functional states.

**Role of AVR$_{A13}$-V2 in the breakdown of *Mla13* resistance in the European *Bgh* population**

Evasion of NLR-mediated pathogen recognition is usually mediated by diversification of the pathogen's effector repertoire, including allelic variation of effector genes that results in abrogation of effector-NLR receptor associations. This model applies to the virulent variant AVR$_{A13}$-V1. However, AVR$_{A13}$-V2 not only interacts strongly with MLA13, but also inhibits MLA13 cell death signalling in a dominant manner. This raises the possibility that *Bgh* AVR$_{A13}$-V2 facilitates rapid clonal dispersal of virulence in *Bgh* populations that are avirulent on *Mla13*. In the European *Bgh* population the virulence frequency on *Mla13* increased from 0.2% in the 1980s to as high as 60% in 1995 (Gacek, 1987; Jørgensen, J.H.; Hovmøller, 1987; Hovmøller *et al.*, 2000), suggesting a major shift in genetic variation of *AVRa$_{13}$* on a continental scale. By contrast, virulence on *Mla13* barley appears to be low at a global scale, with only 7% of *Bgh* isolates in a global strain collection overcoming *Mla13*-mediated resistance (Lu *et al.*, 2016; Rsaliyev *et al.*, 2017; Saur *et al.*, 2019*a*). In addition, *AVR$_{a13}$/BGH_20990* has a very low frequency of non-synonymous SNPs in tested global and local *Bgh* populations (0.9 non-synonymous SNPs/100 bp coding sequence), indicating an overall low genetic diversity of *AVR$_{a13}$* (Saur *et al.*, 2019*a*). Our data demonstrate a dominant negative activity of *AVR$_{A13}$*-V2 on MLA13 therefore suggesting that the breakdown of *Mla13* resistance was caused by direct manipulation of the receptor activation mechanism rather than by evasion of MLA13 recognition.

## Materials and methods

### *Plant and fungal materials and growth conditions*

Near isogenic lines (NILs) of the barley cultivar Manchuria were grown at 19 °C, 70% relative humidity, and under a 16 h photoperiod. *N. benthamiana* plants were grown under standard greenhouse conditions under a 16 h photoperiod. Maintenance of *Bgh* isolates was carried out as described previously (Lu *et al.*, 2016).

### *Generation of expression constructs*

For transient gene expression assays in *N. benthamiana* and barley protoplasts and for yeast 2-hybrid interaction studies, coding sequences of receptor and effector genes with or without stop codons were either synthesized as pDONR221 entry clones from GeneArt (Thermo Scientific), or were published previously (Saur *et al.*, 2019*a*). Respective genes were transferred from entry or donor vectors into the expression vectors pIPKb002 (Himmelbach *et al.*, 2007), pGWB414, pGWB517 (Nakagawa *et al.*, 2007), pXCSG-GW-HA, pXCSG-GW-Myc, pXCSG-GW-mYFP (Garcia *et al.*, 2010), pAMpAT-GW-BirA-4Myc, pLexA-GW, or pB42AD-GW (Shen *et al.*, 2007) as indicated using LR Clonase II (Thermo Scientific).

### *Transient gene expression by Agrobacterium-mediated transformation of Nicotiana benthamiana leaves*

*Agrobacterium tumefaciens* GV3101:pMP90K were freshly transformed with respective constructs of interest and grown from single colonies in liquid Luria broth medium containing appropriate antibiotics for ~ 24 hours at 28 °C to an $OD_{600}$ not higher than 1.5. Bacterial cells were harvested by centrifugation at 2500 × *g* for 15 min followed by resuspension in infiltration medium (10 mM MES, pH 5.6, 10 mM $MgCl_2$, and 200 µM acetosyringone) to a final $OD_{600}$ = 1. Cultures were incubated for two to four h at 28 °C with 180 rpm shaking before infiltration into leaves from three to five-week-old *N. benthamiana* plants. For co-expression of multiple constructs, Agrobacteria carrying the genes of interest were mixed equally unless indicated otherwise. Cell death was assessed one to five days post infiltration as

indicated and tissue for immunodetection analysis was harvested one to two days post infiltration as indicated.

***Protein extraction from Nicotiana benthamiana leaf tissue for protein detection by immunoblotting***

Frozen leaf material was ground to a fine powder using pre-cooled adapters in a bead beater (Retsch) and thawed in cold plant protein extraction buffer (150 mM Tris-HCl, pH 7.5, 150 mM NaCl, 10 mM EDTA, 10% (v/v) glycerol, 5 mM DTT, 2% (v/v) plant protease inhibitor cocktail (Sigma), 1 mM PMSF, and 0.5 % (v/v) IGEPAL) at a ratio of 50 mg fresh tissue/150 µl of extraction buffer. Extracts were centrifuged twice at 15,000 × *g* for 10 min at 4 °C. For SDS-PAGE, extracts were diluted 4:1 with 4x SDS loading buffer and heated to 85 °C for 10 to 15 min before again removing insoluble material by centrifugation at 15,000 × *g* for 5 min. For pull-down of mYFP-tagged proteins, GFP-Trap-MA (Chromotek) beads were incubated in equilibration buffer for 1 h at 4 °C and subsequently mixed with one ml of protein extracts for 2 to 3 h at 4 °C with slow but constant rotation. Then, conjugated GFP-Trap beads were washed five times in 1 ml of cold wash buffer at 4 °C before interacting proteins were stripped from the beads by boiling in 25 µl of 4x SDS loading buffer for 5 min. Samples were separated on 8% to 13% SDS-PAGE gels, blotted onto PVDF membrane, and probed with anti-GFP (abcam ab6556), anti-Myc (abcam ab9106) or anti-HA (Roche 3F10) followed by anti-rabbit IgG-HRP (Santa Cruz Biotechnology sc-2313) or anti-rat IgG-HRP (abcam ab97057) secondary antibodies. Epitope-tagged proteins were detected by the HRP activity on SuperSignal West Femto Maximum Sensitivity Substrate (Thermo Fisher 34095) using a Gel Doc™ XR+ Gel Documentation System (Bio-Rad).

***Proximity-dependent protein labelling of proteins transiently expressed in Nicotiana benthamiana leaves.***

Pull-down of biotinylated proteins was performed by following published protocols (Conlan *et al.*, 2018) with the alteration that free biotin was not removed before adding streptavidin to protein extracts. Instead, we applied a 10 µM biotin solution to the plant tissue (instead of a 75 µM solution (Conlan et al., 2018). We followed a sequence of infiltrations to minimise MLA-mediated cell death of

505 *N. benhamiana* leaf tissue: *Agrobacterium tumefaciens* GV3101::pMP90K carrying *35S:Mla-4Myc*
506 constructs were grown from glycerol stocks and infiltrated (day 1). At 24 h post infiltration of the *Mla*
507 constructs, Agrobacteria freshly transformed with *35S:AVR$_{a13}$-BirA-4Myc* constructs or *EV* were
508 infiltrated as indicated (day 2). Ten µM of free biotin in infiltration buffer lacking acetosyringone was
509 infiltrated at 24 h after the second infiltration and 48 h after the first infiltration (day 3). Tissue for
510 streptavidin-based precipitation of biotinylated proteins was harvested 24 h post infiltration of free
511 biotin. Frozen leaf material was ground to a fine powder using pre-cooled adapters in a bead beater
512 (Retsch) and thawed in cold plant denaturing extraction buffer (150 mM Tris-HCl, pH 7.5, 150 mM NaCl,
513 10 mM EDTA, 5% (v/v) glycerol, 5 mM DTT, 1% (v/v) plant protease inhibitor cocktail (Sigma), 1 mM
514 NaF, 1 mM sodium orthovanadate, 1 mM PMSF, 1% TritonX-100 and 0.5 % (w/v) SDS) at a ratio of 300
515 mg fresh tissue/2 ml of denaturing extraction buffer. Extracts were incubated rotating at 4°C for 30
516 minutes before the removal of insoluble material by centrifugation at 21,000 × g for 30 min at 4 °C.
517 Streptavidin coated Dynabeads (100 µL/sample, MyOne streptavidin C1, Thermo Fisher) were
518 incubated in wash buffer (150 mM Tris-HCl, pH 7.5, 150 mM NaCl, 10 mM EDTA, 5% (v/v) glycerol, 1%
519 (v/v) plant protease inhibitor cocktail (Sigma)) containing 1% BSA for 1 h at 4 °C and subsequently
520 mixed with 2two ml of protein extracts for 3 h at 4 °C with slow but constant rotation. Then, conjugated
521 Streptavidin beads were washed four times in 1 ml of cold wash buffer before interacting proteins
522 were stripped from the beads by heating to 85°C for 10-15 min in 50 µl of 4x SDS loading buffer. From
523 these 50 µl, 30µl were loaded on 9% SDS-PAGE gels. Proteins were blotted onto PVDF membrane and
524 probed with anti-Myc (abcam ab9106) followed by anti-rabbit IgG-HRP (Santa Cruz Biotechnology sc-
525 2313) secondary antibodies. Myc-tagged proteins were detected by the HRP activity on SuperSignal
526 West Femto Maximum Sensitivity Substrate (Thermo Fisher 34095) using a Gel Doc™ XR+ Gel
527 Documentation System (Bio-Rad).

528 ***Transient gene expression and cell death assay in barley protoplasts***

529 Assessment of protoplast cell death using a luciferase activity as a proxy for cell viability was performed
530 as described (Saur *et al.*, 2019*b*). Briefly, *AVR$_{a13}$ -V2* cDNA lacking the respective signal peptide was

expressed from the Zea mays ubiquitin promotor in protoplasts isolated from barley cultivar Manchuria CI 2330 and cultivar Manchuria *Mla13* NIL CI 16155. For this, the epidermis of the primary leaves from seven to eight-day-old plants was removed before leaves were immersed in the enzyme solution. A total volume of 30 µl water containing 5 µg of the *luciferase* reporter and 6 µg of the $AVR_{a13}$-*V2* effector construct or an *EV* was transfected into 300 µL barley protoplasts at a concentration of 5 × $10^5$ protoplasts/ml solution. Protoplasts were recovered in regeneration buffer supplemented with $LaCl_3$ as indicated. About 16 h after transfection, protoplasts were collected by centrifugation at 1000 × *g*, the supernatant was discarded, and 200 µl 2x cell culture lysis buffer were added (Promega, E1531). Luciferase activity was determined by mixing 50 µl of protoplast lysate with 50 µl luciferase substrate (Promega, E1501) in a white 96-well plate and light emission was measured at 1 second/well using a microplate luminometer (Centro, LB960).

***Protein extraction from barley protoplasts and fusion protein detection by immunoblotting***

To determine the effect of $LaCl_3$ treatment on $AVR_{A13}$ protein, for each $LaCl_3$ treatment, 300 µg of the $AVR_{a13}$-*V2-mYFP* effector construct or an *EV* was transfected into 3 ml pf barley protoplasts cultivar Manchuria CI 2330 at a concentration of 5 × $10^5$ protoplasts/ml solution. Protoplasts were recovered in regeneration buffer supplemented with the $LaCl_3$ to the final concentrations indicated. About 16 h post transfection, protoplasts were collected by centrifugation at 1000 × *g*, the supernatant was discarded and protoplast pellets were frozen in liquid nitrogen. Total protein was extracted by the addition of 100 µl cold plant protein extraction buffer (200 mM Tris-HCl, pH 7.5, 150 mM NaCl, 10 mM EDTA, 10% (v/v) glycerol, 12 mM DTT, 2% (v/v) plant protease inhibitor cocktail (Sigma), and 1 % (v/v) IGEPAL) to each protoplast pellet. Extracts were centrifuged at 15,000 × *g* for 5 min at 4 °C. For SDS-PAGE, extracts were diluted 4:1 with 4x SDS loading buffer and heated to 85 °C for 10 to 15 min before removing insoluble material by centrifugation at top speed for 5 minutes. Samples were separated on 10% SDS-PAGE gels, blotted onto PVDF membrane, and probed with anti-GFP (Santa Cruz Biotechnology sc-8334 or abcam ab6556) followed by anti-rabbit IgG-HRP (Santa Cruz Biotechnology sc-2313) secondary antibodies. mYFP tagged proteins were detected by the HRP activity on SuperSignal

557 West Femto Maximum Sensitivity Substrate (Thermo Fisher 34095) using a Gel Doc™ XR+ Gel
558 Documentation System (Bio-Rad).

559 ***Yeast 2-hybrid assay and yeast protein extraction***

560 *NLR* receptor gene variants were cloned into the pLexA-GW vector (Shen *et al.*, 2007) for expression
561 with an N-terminal LexA activation domain under the control of a constitutive ADH1 promoter (BD-
562 NLR). Effector variants were cloned into pB42AD-GW (Shen *et al.*, 2007) for expression with an N-
563 terminal B42 activation domain followed by the HA-tag under the control of an inducible GAL1
564 promoter (AD-AVR). Using the lithium acetate method (Gietz and Woods, 2002), bait and prey
565 constructs were co-transformed into the yeast strain EGY4.8 p8op and successful transformants were
566 selected by colony growth on SD-UHW/Glu (2% (w/v) Glucose, 0.139% (w/v) yeast synthetic drop-out
567 medium pH 6 without uracil, histidine, tryptophan, 0.67% (w/v) BD Difco yeast nitrogen base, 2% (w/v)
568 Bacto Agar). Yeast transformants were grown to $OD_{600}$ = 1 in liquid SD-UHW/Glu before harvesting cells
569 for drop out of the dilution series on SD-UHW/Gal/Raf media (SD-UHW without glucose but with 2%
570 (w/v) Galactose 1 % (w/v) Raffinose, with (-UHW) or without Leucine (-UHWL)) and incubated for one
571 to two weeks at 30 °C.

572 For protein detection, yeast strains were grown to $OD_{600}$ = 1 in SD-UHW/Gal/Raf liquid medium at 30 °C
573 and 200 rpm shaking, and proteins were extracted using 200 mM NaOH (NaOH method) (Zhang *et*
574 *al.*, 2011)). Total protein samples were separated on 9% or 12% SDS-PAGE gels, blotted onto PVDF
575 membrane, and probed with anti-HA (Merck, clone 3F10) or anti-LexA (Santa Cruz Biotechnology,
576 sc7544) primary antibodies followed by anti-rat (Santa Cruz Biotechnology, sc2065) or anti-mouse IgG-
577 HRP (Santa Cruz Biotechnology, sc2005) secondary antibodies as appropriate. HA and LexA fusion
578 proteins were detected by HRP activity on SuperSignal West Femto Maximum Sensitivity Substrate
579 (Thermo Fisher 34095) using a Gel Doc™ XR+ Gel Documentation System (Bio-Rad).

580

581

582 **Supplement**

583 **Figure S1:** Proximity-dependent protein labelling confirms requirement of $AVR_{A13}$ C-terminus for
584 MLA13 interaction.

585 **Figure S2:** Specificity control to Fig. 1D.

586 **Figure S3:** Gain-of-function and loss-of-function NLR mutants and their ability to bind matching
587 avirulence effectors.

588 **Figure S4:** Schematic model of MLA13 wild-type and mutant conformations.

589 **Figure S5:** Schematic models of MLA13 activation by *Bgh* $AVR_{A13}$ -1 and inhibition by $AVR_{A13}$-V2,
590 respectively.

591 **Supplemental Raw Data:** raw data of all figures.

592

593 ## Acknowledgements

594 We would like to thank Sabine Haigis and Petra Köchner for technical support and maintenance of *Bgh*
595 isolates and Ksenia Krasileva for critical comments on the manuscript. Although the resulting crosses
596 could not be assessed for *Bgh* infection due to loss of MLA13 resistance in control lines, we highly
597 acknowledge the group of Matthew Moscou that crossed *Mla13* barley with *$AVR_{a13}$-V2* transgenic lines
598 for assessing $AVR_{A13}$-V2-mediated inhibition of Mla13 resistance. IMLS, TM and PSL acknowledge
599 support from the Cluster of Excellence on Plant Sciences (CEPLAS) funded by the Deutsche
600 Forschungsgemeinschaft (DFG, German Research Foundation) under Germany's Excellence Strategy –
601 EXC 2048/1 – Project ID: 390686111 and funding from the DFG Collaborative Research Centre Project-
602 ID 414786233 (SFB 1403). This work was also funded by the DFG Emmy Noether Programme (SA
603 4093/1-1 to IMLS), the Daimler and Benz Foundation (IMLS) and the Max Planck Society (PSL).

604

605

## Author contributions

EEC, MBS, TM, PSL & IMLS designed the research, EEC, MBS and IMLS performed the experiments and data analysis. EEC, IMLS and PSL wrote the paper with contributions from all authors.

## Conflict of interest

The authors declare no conflict of interest.

## Data availability

All relevant data are available within the paper and its supplementary data published online.

## References

**Adachi H, Contreras MP, Harant A, *et al.*** 2019. An N-terminal motif in NLR immune receptors is functionally conserved across distantly related plant species. Elife **8**, eLife.49956.

**Bai SW, Liu J, Chang C, *et al.*** 2012. Structure-Function Analysis of Barley NLR Immune Receptor MLA10 Reveals Its Cell Compartment Specific Activity in Cell Death and Disease Resistance. Plos Pathogens **8**, e1002752.

**Bauer S, Yu D, Lawson AW, Saur IM, Frantzeskakis L, Kracher B, Logemann E, Chai J, Maekawa T, Schulze-Lefert P**. 2021. The leucine-rich repeats in allelic barley MLA immune receptors define specificity towards sequence-unrelated powdery mildew avirulence effectors with a predicted common RNase-like fold. PLOS Pathogens **17**, e1009223.

**Bendahmane A, Farnham G, Moffett P, Baulcombe DC**. 2002. Constitutive gain-of-function mutants in a nucleotide binding site-leucine rich repeat protein encoded at the Rx locus of potato. Plant Journal **32**, 195–204.

**Bernoux M, Burdett H, Williams SJ, *et al.*** 2016. Comparative Analysis of the Flax Immune Receptors L6 and L7 Suggests an Equilibrium-Based Switch Activation Model. Plant Cell **28**, 146–159.

**Bernoux M, Ve T, Williams S, Warren C, Hatters D, Valkov E, Zhang XX, Ellis JG, Kobe B, Dodds PN**. 2011. Structural and Functional Analysis of a Plant Resistance Protein TIR Domain Reveals Interfaces for Self-Association, Signaling, and Autoregulation. Cell Host & Microbe **9**, 200–211.

**Bettgenhaeuser J, Hernández-Pinzón I, Dawson AM, *et al.*** 2021. The barley immune receptor Mla recognizes multiple pathogens and contributes to host range dynamics. Nature Communications **12**, 6915.

**Bi G, Su M, Li N, *et al.*** 2021. The ZAR1 resistosome is a calcium-permeable channel triggering plant immune signaling. Cell **184**, 3528-3541.e12.

**Brabham HJ, Cruz DGD la, Were V, *et al.*** 2022. Barley MLA3 recognizes the host-specificity determinant PWL2 from rice blast (M. oryzae). bioRxiv, doi:10.1101/2022.10.21.512921.

**Burdett H, Bentham AR, Williams SJ, Dodds PN, Anderson PA, Banfield MJ, Kobe B**. 2019. The Plant 'Resistosome': Structural Insights into Immune Signaling. Cell Host & Microbe **26**, 193–201.

**Cesari S**. 2018. Multiple strategies for pathogen perception by plant immune receptors. New Phytologist **219**, 17–24.

**Chen J, Upadhyaya NM, Ortiz D, *et al.*** 2017. Loss of AvrSr50 by somatic exchange in stem rust leads to virulence for Sr50 resistance in wheat. Science **358**, 1607–1610.

**Collier SM, Hamel LP, Moffett P**. 2011. Cell Death Mediated by the N-Terminal Domains of a Unique and Highly Conserved Class of NB-LRR Protein. Molecular Plant-Microbe Interactions **24**, 918–931.

**Conlan B, Stoll T, Gorman JJ, Saur I, Rathjen JP**. 2018. Development of a Rapid in planta BioID System as a Probe for Plasma Membrane-Associated Immunity Proteins. Frontiers in Plant Science **9**, 1882.

**Dinesh-Kumar SP, Baker BJ**. 2000. Structure-function analysis of the tobacco mosaic virus resistance gene N. Proceedings of the National Academy of Sciences USA **97**, 14789–94.

**Dodds PN, Lawrence GJ, Catanzariti AM, Teh T, Wang CIA, Ayliffe MA, Kobe B, Ellis JG**. 2006. Direct protein interaction underlies gene-for-gene specificity and coevolution of the flax resistance genes

and flax rust avirulence genes. Proceedings of the National Academy of Sciences USA **103**, 8888–8893.

**Dodds PN, Rathjen JP**. 2010. Plant immunity: towards an integrated view of plant-pathogen interactions. Nature Reviews Genetics **11**, 539–548.

**Förderer A, Li E, Lawson AW, *et al.*** 2022*a*. A wheat resistosome defines common principles of immune receptor channels. 532 | Nature | **610**.

**Förderer A, Yu D, Li E, Chai J**. 2022*b*. Resistosomes at the interface of pathogens and plants. Current Opinion in Plant Biology **67**, 102212.

**Gacek E**. 1987. Distribution of barley powdery mildew resistance and virulence in Poland 1984-1986. Advances in agricultural biotechnology, 93–98.

**Gao Z, Chung EH, Eitas TK, Dangl JL**. 2011. Plant intracellular innate immune receptor Resistance to Pseudomonas syringae pv. maculicola 1 (RPM1) is activated at, and functions on, the plasma membrane. Proceedings of the National Academy of Sciences USA **108**, 7619–7624.

**Garcia A v, Blanvillain-Baufume S, Huibers RP, Wiermer M, Li GY, Gobbato E, Rietz S, Parker JE**. 2010. Balanced Nuclear and Cytoplasmic Activities of EDS1 Are Required for a Complete Plant Innate Immune Response. Plos Pathogens **6**, e1000970.

**Gietz RD, Woods RA**. 2002. Transformation of yeast by lithium acetate/single-stranded carrier DNA/polyethylene glycol method. Guide to Yeast Genetics and Molecular and Cell Biology, **350**, 87–96.

**Glawe DA**. 2008. The powdery mildews: A review of the world's most familiar (yet poorly known) plant pathogens. Annual Review of Phytopathology **46**, 27–51.

**Grant M, Brown I, Adams S, Knight M, Ainslie A, Mansfield J**. 2000. The RPM1 plant disease resistance gene facilitates a rapid and sustained increase in cytosolic calcium that is necessary for the oxidative burst and hypersensitive cell death. Plant Journal **23**, 441–450.

**Himmelbach A, Zierold U, Hensel G, Riechen J, Douchkov D, Schweizer P, Kumlehn J**. 2007. A set of modular binary vectors for transformation of cereals. Plant Physiology **145**, 1192–1200.

**Horsefield S, Burdett H, Zhang XX, *et al.*** 2019. NAD(+) cleavage activity by animal an plant TIR domains in cell death pathways. Science **365**, 793–799.

**Hovmøller MS, Caffier V, Jalli M, *et al.*** 2000. Plant Genetics and Breeding The European barley powdery mildew virulence survey and disease nursery 1993-1999. Agronomie, EDP Sciences, **20**, 729–743.

**Howles P, Lawrence G, Finnegan J, McFadden H, Ayliffe M, Dodds P, Ellis J**. 2005. Autoactive alleles of the flax L6 rust resistance gene induce non-race-specific rust resistance associated with the hypersensitive response. Molecular plant-microbe interactions : MPMI **18**, 570–582.

**Huang S, Jia A, Song W, *et al.*** 2022. Identification and receptor mechanism of TIR-catalyzed small molecules in plant immunity. Science **377**.

**Jacob P, Kim NH, Wu F, *et al.*** 2021. Plant "helper" immune receptors are calcium ion-permeable nonselective cation channels. Science **373**, 420–425.

**Jia A, Huang S, Song W, *et al.*** 2022. TIR-catalyzed ADP-ribosylation reactions produce signaling molecules for plant immunity. Science **377**, eabq8180.

**Jia Y, McAdams SA, Bryan GT, Hershey HP, Valent B**. 2000. Direct interaction of resistance gene and avirulence gene products confers rice blast resistance. The EMBO journal **19**, 4004–4014.

**Jones JDG, Vance RE, Dangl JL**. 2016. Intracellular innate immune surveillance devices in plants and animals. Science **354**.

**Jorgensen JH**. 1994. Genetics of Powdery Mildew Resistance in Barley. Critical Reviews in Plant Sciences **13**, 97–119.

**Jørgensen, J.H.; Hovmøller MStøvring**. 1987. Distribution of Powdery Mildew Resistance and Virulence in Denmark - Research - Aarhus University. Integrated control to reduce damage caused by cereal mildews., 43–47.

**Jubic LM, Saile S, Furzer OJ, el Kasmi F, Dangl JL**. 2019. Help wanted: helper NLRs and plant immune responses. Current opinion in plant biology **50**, 82–94.

**de la Concepcion JC, Franceschetti M, Maqbool A, Saitoh H, Terauchi R, Kamoun S, Banfield MJ**. 2018. Polymorphic residues in rice NLRs expand binding and response to effectors of the blast pathogen. Nature Plants **4**, 576–585.

**Lapin D, Kovacova V, Sun X, *et al.*** 2019. A coevolved EDS1-SAG101-NRG1 module mediates cell death signaling by TIR-domain immune receptors. Plant Cell.

**Lu XL, Kracher B, Saur IML, Bauer S, Ellwood SR, Wise R, Yaeno T, Maekawa T, Schulze-Lefert P**. 2016. Allelic barley MLA immune receptors recognize sequence-unrelated avirulence effectors of the powdery mildew pathogen. Proceedings of the National Academy of Sciences USA **113**, 6486–6495.

**Maekawa T, Cheng W, Spiridon LN, *et al.*** 2011*a*. Coiled-coil domain-dependent homodimerization of intracellular barley immune receptors defines a minimal functional module for triggering cell death. Cell Host and Microbe **9**, 187–199.

**Maekawa T, Kashkar H, Coll NS**. 2022. Dying in self-defence: a comparative overview of immunogenic cell death signalling in animals and plants. Cell Death & Differentiation **Epub ahead**.

**Maekawa T, Kracher B, Saur I, Yoshikawa-Maekawa M, Kellner R, Pankin A, von Korff M, Schulze-Lefert P**. 2019. Subfamily-Specific Specialization of RGH1/MLA Immune Receptors in Wild Barley. Molecular Plant-Microbe Interactions **32**, 107–119.

**Maekawa T, Kufer TA, Schulze-Lefert P**. 2011*b*. NLR functions in plant and animal immune systems: so far and yet so close. Nature Immunology **12**, 818–826.

**Mago R, Zhang P, Vautrin S, *et al.*** 2015. The wheat Sr50 gene reveals rich diversity at a cereal disease resistance locus. Nature Plants **1**, 15186.

**Ma S, Lapin D, Liu L, *et al.*** 2020. Direct pathogen-induced assembly of an NLR immune receptor complex to form a holoenzyme. Science **370**, eabe3069.

**Märkle H, Saur IML, Stam R**. 2022. Evolution of resistance (R) gene specificity. Essays in biochemistry **66**, 551–560.

**Martin R, Qi T, Zhang H, Liu F, King M, Toth C, Nogales E, Staskawicz BJ**. 2020. Structure of the activated ROQ1 resistosome directly recognizing the pathogen effector XopQ. Science **370**, abd9993.

**Moseman JG, Schaller CW**. 1960. Genetics of the allelic aeries at the Mla locus in barley and cultures of Erysiphe graminis f. sp. hordei that differentiate these alleles. Phytopathology **50**, 736–741.

**Nakagawa T, Kurose T, Hino T, Tanaka K, Kawamukai M, Niwa Y, Toyooka K, Matsuoka K, Jinbo T, Kimura T**. 2007. Development of series of gateway binary vectors, pGWBs, for realizing efficient construction of fusion genes for plant transformation. Journal of Bioscience and Bioengineering **104**, 34–41.

**Nishimura MT, Anderson RG, Cherkis KA, *et al.*** 2017. TIR-only protein RBA1 recognizes a pathogen effector to regulate cell death in Arabidopsis. Proceedings of the National Academy of Sciences USA **114**, E2053–E2062.

**Ntoukakis V, Balmuth AL, Mucyn TS, Gutierrez JR, Jones AME, Rathjen JP**. 2013. The Tomato Prf Complex Is a Molecular Trap for Bacterial Effectors Based on Pto Transphosphorylation. PLOS Pathogens **9**, e1003123.

**Ntoukakis V, Saur IML, Conlan B, Rathjen JP**. 2014. The changing of the guard: the Pto/Prf receptor complex of tomato and pathogen recognition. Current opinion in plant biology **20**, 69–74.

**Ortiz D, Chen J, Outram MA, *et al.*** 2022. The stem rust effector protein AvrSr50 escapes Sr50 recognition by a substitution in a single surface-exposed residue. New Phytologist **234**, 592–606.

**Ortiz D, de Guillen K, Cesari S, Chalvon V, Gracy J, Padilla A, Kroj T**. 2017. Recognition of the Magnaporthe oryzae Effector AVR-Pia by the Decoy Domain of the Rice NLR Immune Receptor RGA5. Plant Cell **29**, 156–168.

**Paulmurugan R, Umezawa Y, Gambhir SS**. 2002. Noninvasive imaging of protein-protein interactions in living subjects by using reporter protein complementation and reconstitution strategies. Proceedings of the National Academy of Sciences USA **99**, 15608–15613.

**Periyannan S, Moore J, Ayliffe M, *et al.*** 2013. The Gene Sr33, an Ortholog of Barley Mla Genes, Encodes Resistance to Wheat Stem Rust Race Ug99. Science **341**, 786–788.

**Rairdan GJ, Moffett P**. 2006. Distinct Domains in the ARC Region of the Potato Resistance Protein Rx Mediate LRR Binding and Inhibition of Activation. The Plant Cell **18**, 2082–2093.

**Roberts M, Tang S, Stallmann A, Dangl JL, Bonardi V**. 2013. Genetic Requirements for Signaling from an Autoactive Plant NB-LRR Intracellular Innate Immune Receptor. PLOS Genetics **9**, e1003465.

**Rsaliyev A, Pahratdinova Z, Rsaliyev S**. 2017. Characterizing the pathotype structure of barley powdery mildew and effectiveness of resistance genes to this pathogen in Kazakhstan. BMC Plant Biology **17**, 178.

**Saile SC, Id PJ, Castel B, *et al.*** 2020. Two unequally redundant 'helper' immune receptor families mediate Arabidopsis thaliana intracellular 'sensor' immune receptor functions. PLOS Biology **18**, e3000783.

**Saur IML, Bauer S, Kracher B, *et al.*** 2019*a*. Multiple pairs of allelic MLA immune receptor-powdery mildew AVRA effectors argue for a direct recognition mechanism. Elife **8**, e44471.

**Saur IML, Bauer S, Lu X, Schulze-Lefert P**. 2019*b*. A cell death assay in barley and wheat protoplasts for identification and validation of matching pathogen AVR effector and plant NLR immune receptors. Plant Methods **15**, doi: 10.1186/s13007-019-0502-0.

**Saur IML, Hückelhoven R**. 2021. Recognition and defence of plant-infecting fungal pathogens. Journal of Plant Physiology **256**, 153324.

**Saur IML, Panstruga R, Schulze-Lefert P**. 2021. NOD-like receptor-mediated plant immunity: from structure to cell death. Nature reviews. Immunology **21**, 305–318.

**Seeholzer S, Tsuchimatsu T, Jordan T, Bieri S, Pajonk S, Yang WX, Jahoor A, Shimizu KK, Keller B, Schulze-Lefert P**. 2010. Diversity at the Mla Powdery Mildew Resistance Locus from Cultivated Barley Reveals Sites of Positive Selection. Molecular Plant-Microbe Interactions **23**, 497–509.

**Shao ZQ, Xue JY, Wu P, Zhang YM, Wu Y, Hang YY, Wang B, Chen JQ**. 2016. Large-scale analyses of angiosperm nucleotide-binding site-leucine-rich repeat genes reveal three anciently diverged classes with distinct evolutionary patterns. Plant Physiology **170**, 2095–2109.

**Shen QH, Saijo Y, Mauch S, Biskup C, Bieri S, Keller B, Seki H, Ulker B, Somssich IE, Schulze-Lefert P**. 2007. Nuclear activity of MLA immune receptors links isolate-specific and basal disease-resistance responses. Science **315**, 1098–1103.

**Shen QH, Zhou FS, Bieri S, Haizel T, Shirasu K, Schulze-Lefert P**. 2003. Recognition specificity and RAR1/SGT1 dependence in barley Mla disease resistance genes to the powdery mildew fungus. The Plant Cell **15**, 732–744.

**Slootweg EJ, Spiridon LN, Roosien J, *et al.*** 2013. Structural determinants at the interface of the ARC2 and leucine-rich repeat domains control the activation of the plant immune receptors Rx1 and Gpa2. Plant physiology **162**, 1510–1528.

**Swiderski MR, Birker D, Jones JDG**. 2009. The TIR Domain of TIR-NB-LRR Resistance Proteins Is a Signaling Domain Involved in Cell Death Induction. Molecular Plant-Microbe Interactions **22**, 157–165.

**Tamborski J, Seong K, Liu F, Staskawicz B, Krasileva K v**. 2022. Engineering of Sr33 and Sr50 plant immune receptors to alter recognition specificity and autoactivity. bioRxiv, 2022.03.05.483131.

**Wan L, Essuman K, Anderson RG, *et al.*** 2019. TIR domains of plant immune receptors are NAD(+)-cleaving enzymes that promote cell death. Science **365**, 799–803.

**Wang JZ, Hu MJ, Wang J, Qi JF, Han ZF, Wang GX, Qi YJ, Wang HW, Zhou JM, Chai JJ**. 2019*a*. Reconstitution and structure of a plant NLR resistosome conferring immunity. Science **364**, eaav5870.

**Wang JZ, Wang J, Hu MJ, *et al.*** 2019*b*. Ligand-triggered allosteric ADP release primes a plant NLR complex. Science **364**, eaav5868.

**Williams SJ, Sohn KH, Wan L, *et al.*** 2014. Structural Basis for Assembly and Function of a Heterodimeric Plant Immune Receptor. Science **344**, 299–303.

**Yu D, Song W, Tan EYJ, *et al.*** 2022. TIR domains of plant immune receptors are 2',3'-cAMP/cGMP synthetases mediating cell death. Cell **185**, 2370-2386.e18.

**Zhang TT, Lei J, Yang HJ, Xu K, Wang R, Zhang ZY**. 2011. An improved method for whole protein extraction from yeast Saccharomyces cerevisiae. Yeast **28**, 795–798.

**Zhao YB, Liu MX, Chen TT, *et al.*** 2022. Pathogen effector AvrSr35 triggers Sr35 resistosome assembly via a direct recognition mechanism. Science Advances **8**, 5108.

## Figures

**Fig. 1: The C-terminus of $AVR_{A13}$ effectors controls interaction with and activation of MLA13. (A)** Amino acid (aa) alignment of $AVR_{A13}$ variants analysed for interaction with MLA13 and inhibition of MLA13-mediated cell death. Signal peptide (SP) residues are underlined; aa in pink and blue highlight the aa variation between $AVR_{A13}$-V2 and $AVR_{A13}$-1, respectively. **(B, C)** *Nicotiana benthamiana* leaves were transformed transiently with *35S:Mla13-4Myc* (pGWB517) with one of the $AVR_{a13}$ variants lacking SPs cloned between the 35S promoter and a C-terminal *mYFP* sequence or *empty vector* (*EV*). **(B)** Cell death was determined three days post transformation and figures shown are representatives of at least nine independent leaves from at least three independent plants. **(C)** Protein stability of the $AVR_{A13}$ variants fused to mYFP corresponding to constructs of B. Leaf tissue was harvested two days post infiltration. Total protein was extracted, separated by gel electrophoresis and probed by anti-GFP western blotting (WB). **(D, E)** Yeast cells were co-transformed with *Mla13* fused N-terminally to the *LexA* binding domain sequence (BD) and $AVR_{a13}$ variants lacking SPs fused N-terminally to the *B42* activation domain (AD) and 1xHA tag sequence as indicated. Growth of transformants was determined on selective growth media containing raffinose and galactose as carbon sources but lacking uracil, histidine and tryptophan (-UHW), and interaction of proteins was determined by leucine reporter activity reflected by growth of yeast on selective media containing raffinose and galactose as carbon sources but lacking uracil, histidine, tryptophan and leucine (-UHWL). Figures shown are representatives of at least three experiments and pictures were taken 6 to 8 days after drop out. (**E**) Protein levels of BD-MLA13 and AD-$AVR_A$ variants corresponding to yeast of D. Yeast transformants were grown in raffinose and galactose containing selective media lacking uracil, tryptophan, and histidine to $OD_{600}$ = 1. Then, cells were harvested, total protein extracted, separated by gel electrophoresis, and western blots (WB) were probed with anti-LexA or anti-HA antibodies as indicated. CBB: Coomassie brilliant blue. (**F**) Cartoon and surface representations for the top rank model of $AVR_{A13}$-1 and $AVR_{A13}$-V2 from AlphaFold2 ($pLDDT_{overall}$= 89, $pLDDT_{L/S119}$ >80). Residues

highlighted in pink correspond to the $AVR_{A13}$-1 C-terminal residues and those in blue correspond to the $AVR_{A13}$-V2 C-terminal residues.

**Fig. 2: $AVR_{A13}$-V2 can act as dominant-negative effector on MLA13.** *Nicotiana benthamiana* leaves were co-transformed transiently with cDNAs of *Mla1* or *Mla7* or *MLA13* (pGWB vectors) with $AVR_{a1}$ or $AVR_{a7}$*-2* or $AVR_{a13}$ or *empty vector* (*EV*) as indicated and either $AVR_{a13}$*-V1* or $AVR_{A13}$*-V2* or *EV* fused to epitope tags as indicated. All constructs were expressed from the 35S promoter. **(A, B)** Cell death was determined three to four days post transformation and **(B)** scored from 0 to 3 based on the cell death scale indicated. All values obtained in at least three independent experiments are indicated by dots, error bars = standard error. Differences between samples were assessed by non-parametric Kruskal-Wallis and subsequent Dunn's tests for each MLA variant. Calculated *P* values were as follows: *Mla1:* $p$=0.824, *Mla7:* $p$=0.551 and *Mla13:* $p$=1.00E-06. Samples marked by identical letters in the plots do not differ significantly ($p<0.05$) in the Tukey test for the corresponding MLA. **(C)** Protein levels corresponding to samples of B. Leaf tissue was harvested two days post infiltration. Total protein was extracted and recovered by GFP-Trap ($AVR_{a1}$ and $AVR_{a7}$-2) separated by gel electrophoresis and probed by anti-HA (MLAs), anti-Myc ($AVR_{A13}$-V2-4xMyc) or anti-GFP ($AVR_{A1}$-mYFP, $AVR_{A7}$-2-mYFP and $AVR_{A13}$-1-mYFP) western blotting (WB) as indicated. CBB: Coomassie brilliant blue.

**Fig. 3: Amino acid exchanges in the nucleotide-binding site of MLA13 compromise $AVR_{A13}$ effector binding. (A, B)** Yeast cells were co-transformed with *Mla13 wt* or mutant variants $Mla13^{D502V}$ (MHD) or *Mla13 K207R* (P-loop) fused N-terminally to the *LexA* binding domain sequence (BD) and $AVR_{a13}$ variants lacking SPs fused N-terminally to the *B42* activation domain (AD) and *1xHA* tag sequence as indicated. **(A)** Growth of transformants was determined on selective growth media containing raffinose and galactose as carbon sources but lacking uracil, histidine and tryptophan (-UHW), and interaction of proteins was determined by leucine reporter activity reflected by growth of yeast on selective media containing raffinose and galactose as carbon sources, but lacking uracil,

histidine, tryptophan and leucine (-UHWL). Figures shown are representatives of at least three experiments and pictures were taken 6 to 8 days after drop out. **(B)** Protein levels of BD-MLA13 variants and AD-$AVR_A$ variants corresponding to yeast of A. Yeast transformants were grown in raffinose and galactose containing selective media lacking uracil, tryptophan, and histidine to $OD_{600}$ = 1. Cells were harvested, total protein extracted, separated by gel electrophoresis, and western blots (WB) were probed with anti-LexA or anti-HA antibodies as indicated. **(C, D)** *Nicotiana benthamiana* leaves were co-transformed transiently with cDNAs of $AVR_{a13}$-*V1* or $AVR_{a13}$-V2 or *empty vector* (*EV*) together with constructs encoding either MLA13 or $MLA13^{D502V}$ (pAM-PAT vector) as indicated and under the control of the 35S promoter sequence at a 2:1 ratio. **(C)** Cell death was determined two (MLA13 MHD) to five days (MLA13) post transformation and scored from 0 to 3 based on the cell death scale indicated. All values obtained in at least three independent experiments are indicated by dots, error bars = standard deviation. Differences between samples were assessed by non-parametric Kruskal-Wallis and subsequent Dunn's tests for each MLA variant. Calculated *P* values were as follows: MLA13: *p*=5E-05, MLA13 MHD*: p*=0.078. Samples marked by identical letters in the plots did not differ significantly (p<0.05) in the Tukey test for the corresponding MLA. **(D)** Protein levels corresponding to samples of C. Leaf tissue was harvested 36 hours post infiltration. Total protein was extracted, separated by gel electrophoresis and probed by anti-Myc (MLAs) or anti-GFP ($AVR_{A13}$-V2) western blotting (WB) as indicated. CBB: Coomassie brilliant blue.

**Fig. 4: Amino acid (aa) exchanges in the coiled-coil (CC) domain de-regulate MLA13 auto-inhibition.** **(A)** Amino acid (aa) changes in MLA13 mutant variants. The D2A_E17A and the F99E variants encode changes in the MLA13 coiled-coil (CC) domain, which spans from aa1 to 160. The K207R, D284A, D502V and H501G variants encode changes in the nucleotide-binding site (NB, aa 161 to 549). The S902F_F935I variants affects the leucine-rich repeats (LRR, aa 550 to 942) which are followed by a short C-terminal amino acids sequence. **(B, C)** *Nicotiana benthamiana* leaves were transformed transiently with cDNAs of one of the *Mla13* variants as indicated (pGWB517 vector) either with or

without *$AVR_{a13}$-1* lacking SPs and fused c-terminally to a *mYFP* sequence. All constructs are under the control of the 35S promotor. **(B)** Cell death was determined three days post transformation; n≥9. **(C)** Protein stability of the MLA variants fused to 4xMyc corresponding to constructs of B. Leaf tissue was harvested two days post infiltration. Total protein was extracted, separated by gel electrophoresis and probed by anti-Myc western blotting (WB) as indicated. **(D, E)** Yeast cells were co-transformed with *Mla13* variants fused N-terminally to the *LexA* binding domain (BD) sequence and *$AVR_{a13}$*-V2 lacking SPs fused N-terminally to the *B42* activation domain (AD) and *1xHA* tag sequence as indicated. Growth of transformants was determined on selective growth media containing raffinose and galactose as carbon sources but lacking uracil, histidine and tryptophan (-UHW), and interaction of proteins was determined by leucine reporter activity reflected by growth of yeast on selective media containing raffinose and galactose as carbon sources but lacking uracil, histidine, tryptophan and leucine (-UHWL). Figures shown are representatives of at least three experiments and pictures were taken 6 to 8 days after drop out. (**E**) Protein levels of BD-MLA13 variants and AD-$AVR_{A13}$-V2 corresponding to yeast of D. Yeast transformants were grown in raffinose and galactose containing selective media lacking uracil, tryptophan, and histidine to $OD_{600}$ = 1. Then, cells were harvested, total protein extracted, separated by gel electrophoresis, and western blots (WB) were probed with anti-LexA or anti-HA antibodies as indicated. CBB: Coomassie brilliant blue. **(F)** *N. benthamiana* leaves were co-transformed transiently with cDNAs of *$AVR_{a13}$-V1*, *$AVR_{a13}$-V2* or *empty vector* (*EV*) together with constructs encoding the MLA13 variant as indicated and under the control of the 35S promoter sequence at a 2:1 ratio. Cell death was determined three days post transformation and scored from 0 to 3 based on the cell death scale indicated. All values obtained in at least two independent experiments are indicated by dots, error bars = standard deviation. Differences between samples were assessed by non-parametric Kruskal-Wallis and subsequent Dunn's tests for each MLA variant. Calculated *P* values were as follows: MLA13*: p* = 9.38E-07, $MLA13^{D2A\_E17A}$: *p* = 0.77. n.s. = no significant difference.

**Fig. 5: Calcium channel activity is required for *Mla13*-mediated cell death in barley (A)** Barley protoplasts of lines CI 16155 (cultivar Manchuria *Mla13*) and CI2330 (Manchuria) were transfected with *pUBQ:luciferase* and piPKb002 containing $AVR_{a13}$*-1* cDNA without signal peptide or a piPKb002 empty vector control and recovered in the presence of $LaCl_3$ at concentrations indicated. Luciferase activity was determined 16 hr post transfection/addition of $LaCl_3$ as a proxy for cell death and normalized against the respective *EV* sample. Error bars = standard deviation. Differences between samples were assessed using non-parametric Kruskal-Wallis and subsequent Dunn's post hoc tests. *p*= 6.179e-10. Samples marked by identical letters in the plot did not differ significantly ($p<0.05$) in Dunn's test. **(B)** Protoplasts derived from cultivar Manchuria CI2330 leaves transfected with *pZmUBQ:*$AVR_{a13}$*-1-mYFP* were harvested 16h post transfection/$LaCl_3$ treatment. Total protein was extracted, separated by gel electrophoresis, and western blots (WB) were probed with anti-GFP antibodies. CBB: Coomassie brilliant blue.

**Figure S1: (A)** *Nicotiana benthamiana* leaves were transformed transiently with cDNAs of the *Mla13* together with *empty vector* (*EV*) or $AVR_{a13}$*-1* lacking SPs and fused c-terminally to *BirA-4Myc* tag sequence and expressed from the 35S promotor. Cell death was determined three days post transformation and picture shows representative of at least three independent leaves. **(B)** *N. benthamiana* leaves were transformed transiently with cDNAs of *Mla1* or *Mla7* or *MLA13* fused C-terminally to a *4xMyc* sequence and at 24 h before re-transformation with cDNAs encoding $AVR_{a13}$*-1-BirA-4xMyc,* $AVR_{a13}$*-V1-BirA-4xMyc,* $AVR_{a13}$*-V2-BirA-4xMyc* or *empty vector* (*EV*) as indicated. All leaves were treated with 10 µM biotin by infiltration at 24h after the second transformation. Leaf tissue was harvested 24h post biotin treatment. Total protein was extracted under denaturing conditions and recovered by Strep IP, separated by gel electrophoresis and probed by anti-Myc western blotting (WB). CBB: Coomassie brilliant blue.

**Fig. S2: Specificity control to Figure 1D. (A,B)** Yeast cells were co-transformed with *Mla1* fused N-terminally to the *LexA* binding domain sequence (BD) and $AVR_{a13}$ variants lacking SPs fused N-terminally to the *B42* activation domain (AD) and 1xHA tag sequence as indicated. Growth of transformants was determined on selective growth media containing raffinose and galactose as carbon sources but lacking uracil, histidine and tryptophan (-UHW), and interaction of proteins was determined by leucine reporter activity reflected by growth of yeast on selective media containing raffinose and galactose as carbon sources but lacking uracil, histidine, tryptophan and leucine (-UHWL). Figures shown are representatives of at least three experiments and pictures were taken 6 to 8 days after drop out. (B) Protein levels of BD-MLA1 and AD-$AVR_A$ variants corresponding to yeast of D. Yeast transformants were grown in raffinose and galactose containing selective media lacking uracil, tryptophan, and histidine to $OD_{600}$ = 1. Then, cells were harvested, total protein extracted, separated by gel electrophoresis, and western blots (WB) were probed with anti-LexA or anti-HA antibodies as indicated. CBB: Coomassie brilliant blue.

**Fig. S3: (A, B)** *Nicotiana benthamiana* leaves were co-transformed transiently with *empty vector* (*EV)* or constructs encoding either MLA13, $MLA13^{K207D}$ or $MLA13^{D502V}$ (pGWB) as indicated with (A) or without (B) cDNA encoding of $AVR_{a13}$*-1* or *EV.* All cDNAs were under the control of the 35S promoter sequence. Cell death was determined three days post transformation. **(C, D)** Yeast cells were co-transformed with Sr50 or $Sr50^{D498V}$ (MHD) fused N-terminally to the *LexA* binding domain sequence (BD) and AvrSr50 variants lacking SPs fused N-terminally to the *B42* activation domain (AD) and 1xHA tag sequence as indicated. Growth of transformants was determined on selective growth media containing raffinose and galactose as carbon sources but lacking uracil, histidine and tryptophan (-UHW), and interaction of proteins was determined by leucine reporter activity reflected by growth of yeast on selective media containing raffinose and galactose as carbon sources but lacking uracil, histidine, tryptophan and leucine (-UHWL). Figures shown are representatives of at least three experiments and pictures were taken 12 to 14 days after drop out. (B) Protein levels of BD-Sr50 and

AD-AvrSr50 variants corresponding to yeast of C. Yeast transformants were grown in raffinose and galactose containing selective media lacking uracil, tryptophan, and histidine to $OD_{600}$ = 1. Then, cells were harvested, total protein extracted, separated by gel electrophoresis, and western blots (WB) were probed with anti-LexA or anti-HA antibodies as indicated. **(E)** *Nicotiana benthamiana* leaves were co-transformed transiently with cDNAs of *$AVR_{a13}$-V1* or *$AVR_{a13}$*-V2 or *empty vector* (*EV*) together with constructs encoding the MLA13 coiled-coil (CC) domain (amino acids (aa) 1-160). **(E)** Cell death was determined two days post transformation and scored from 0 to 3 based on the cell death scale indicated. All values obtained in at least three independent experiments are indicated by dots, error bars = standard error. Differences between samples were assessed by the non-parametric Kruskal-Wallis test. *p*= 0.623871; n.s. = not significant. **(F)** Protein levels corresponding to samples of C. Leaf tissue was harvested 36 hours post infiltration. Total protein was extracted, separated by gel electrophoresis and probed by anti-Myc (MLA13_CC) or anti-GFP ($AVR_{A13}$-V2) western blotting as indicated. CBB: Coomassie brilliant blue.

**Fig. S4:** Schematic models of monomeric and oligomeric MLA13 wild-type, $MLA13^{P\text{-}loop}$, $MLA13^{MHD}$ and $MLA13^{D2A\_E17A}$ conformations with indication of putative effector (purple) entry sites and binding of ADP (green) or ATP (blue).

**Fig. S5:** Schematic models of MLA13 during the multistep process of putative resistosome formation initiated by the interaction with *Bgh* $AVR_{A13}$-1 (A) and putative models for the inhibition of the activation process by $AVR_{A13}$-V2 (B). (**A**) $AVR_{A13}$-1 binding to the effector entry point involving the MLA13 Leucine-rich-repeats (LRR) domain leads to a steric clash and subsequent replacement of adenosine diphosphate (ADP) by adenosine triphosphate ATP) in the nucleotide-binding (NB) pocket of the MLA13. ATP-binding causes additional structural rearrangement of the N-terminal Coiled-coil (CC) domain releasing the α1-helix. In the resulting putative pentameric wheel-like MLA13

resistosome, the α1-helices are thought to form a funnel like structure. (**B**) $AVR_{A13}$-V2 binding is likely either incapable to inducing a steric clash or prevents subsequent release of the α1-helix.

# Figure 1

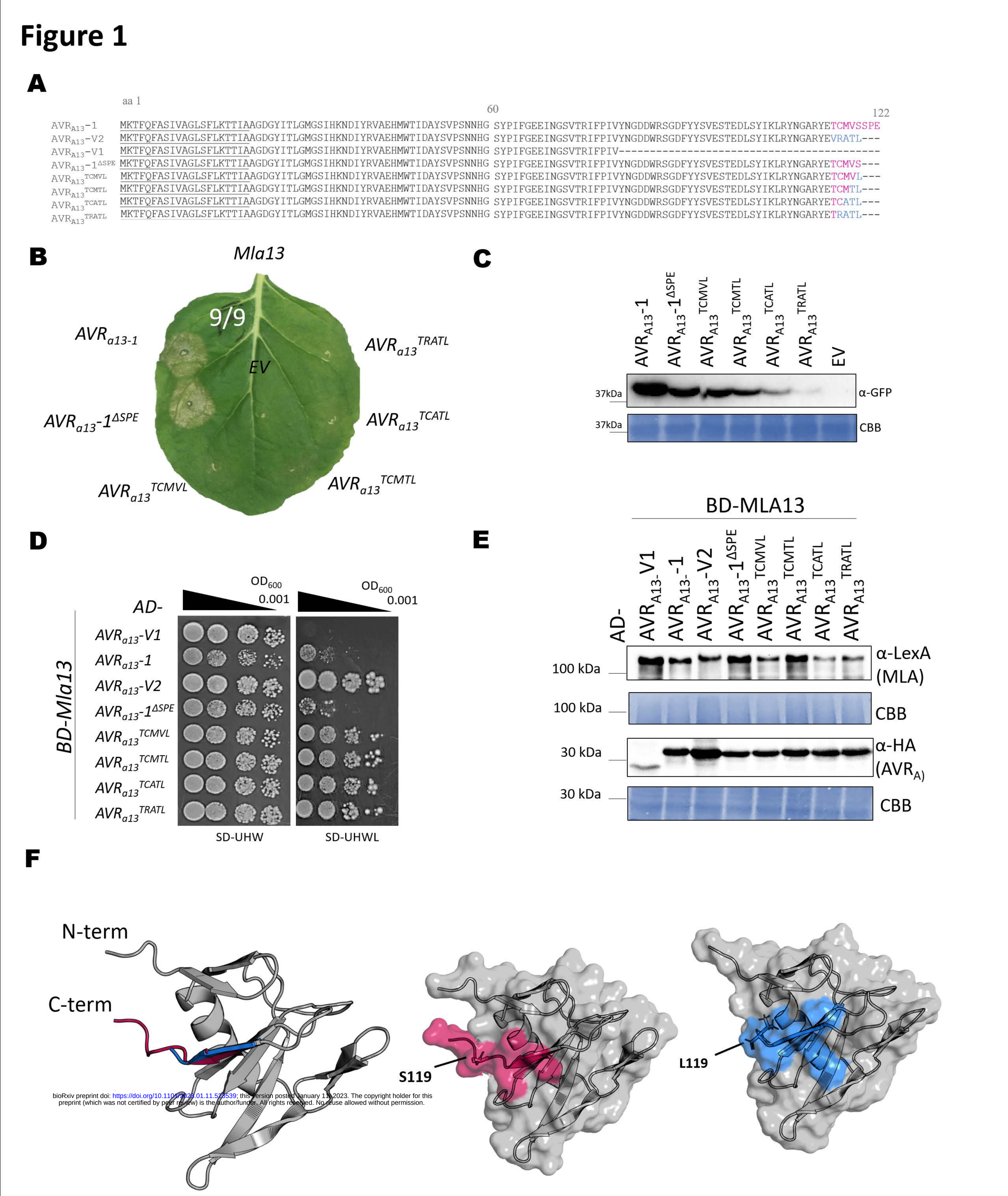




**Fig. 1: The C-terminus of AVR$_{A13}$ effectors controls interaction with and activation of MLA13. (A)** Amino acid (aa) alignment of AVR$_{A13}$ variants analysed for interaction with MLA13 and inhibition of MLA13-mediated cell death. Signal peptide (SP) residues are underlined; aa in pink and blue highlight the aa variation between AVR$_{A13}$-V2 and AVR$_{A13}$-1, respectively. **(B, C)** *Nicotiana benthamiana* leaves were transformed transiently with *35S:Mla13-4Myc* (pGWB517) with one of the *AVR$_{a13}$* variants lacking SPs cloned between the 35S promoter and a C-terminal *mYFP* sequence or *empty vector* (*EV*). **(B)** Cell death was determined three days post transformation and figures shown are representatives of at least nine independent leaves from at least three independent plants. **(C)** Protein stability of the AVR$_{A13}$ variants fused to mYFP corresponding to constructs of B. Leaf tissue was harvested two days post infiltration. Total protein was extracted, separated by gel electrophoresis and probed by anti-GFP western blotting (WB). **(D, E)** Yeast cells were co-transformed with *Mla13* fused N-terminally to the *LexA* binding domain sequence (BD) and *AVR$_{a13}$* variants lacking SPs fused N-terminally to the *B42* activation domain (AD) and 1xHA tag sequence as indicated. Growth of transformants was determined on selective growth media containing raffinose and galactose as carbon sources but lacking uracil, histidine and tryptophan (-UHW), and interaction of proteins was determined by leucine reporter activity reflected by growth of yeast on selective media containing raffinose and galactose as carbon sources but lacking uracil, histidine, tryptophan and leucine (-UHWL). Figures shown are representatives of at least three experiments and pictures were taken 6 to 8 days after drop out. (**E**) Protein levels of BD-MLA13 and AD-AVR$_{A}$ variants corresponding to yeast of D. Yeast transformants were grown in raffinose and galactose containing selective media lacking uracil, tryptophan, and histidine to OD$_{600}$ = 1. Then, cells were harvested, total protein extracted, separated by gel electrophoresis, and western blots (WB) were probed with anti-LexA or anti-HA antibodies as indicated. CBB: Coomassie brilliant blue. (**F**) Cartoon and surface representations for the top rank model of AVR$_{A13}$-1 and AVR$_{A13}$-V2 from AlphaFold2 (pLDDT$_{overall}$= 89, pLDDT$_{L/S119}$ >80). Residues highlighted in pink correspond to the AVR$_{A13}$-1 C-terminal residues and those in blue correspond to the AVR$_{A13}$-V2 C-terminal residues.

# Figure 2

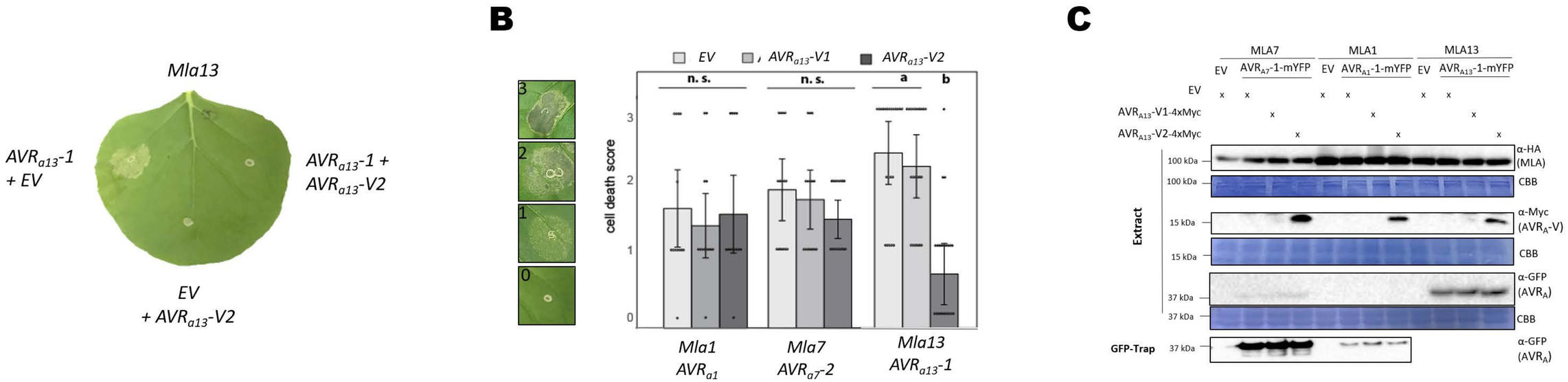


**Fig. 2: $AVR_{A13}$-V2 can act as dominant-negative effector on MLA13.** *Nicotiana benthamiana* leaves were co-transformed transiently with cDNAs of *Mla1* or *Mla7* or *MLA13* (pGWB vectors) with $AVR_{a1}$ or $AVR_{a7}$-*2* or $AVR_{a13}$ or *empty vector* (*EV*) as indicated and either $AVR_{a13}$-*V1* or $AVR_{A13}$-*V2* or *EV* fused to epitope tags as indicated. All constructs were expressed from the 35S promoter. **(A, B)** Cell death was determined three to four days post transformation and **(B)** scored from 0 to 3 based on the cell death scale indicated. All values obtained in at least three independent experiments are indicated by dots, error bars = standard error. Differences between samples were assessed by non-parametric Kruskal-Wallis and subsequent Dunn tests for each MLA variant. Calculated *P* values were as follows: *Mla1: p*=0.824, *Mla7: p*=0.551 and *Mla13: p*=1.00E-06. Samples marked by identical letters in the plots do not differ significantly (p<0.05) in the Tukey test for the corresponding MLA. **(C)** Protein levels corresponding to samples of B. Leaf tissue was harvested two days post infiltration. Total protein was extracted and recovered by GFP-Trap ($AVR_{a1}$ and $AVR_{a7}$-2) separated by gel electrophoresis and probed by anti-HA (MLAs), anti-Myc ($AVR_{A13}$-V2-4xMyc) or anti-GFP ($AVR_{A1}$-mYFP, $AVR_{A7}$-2-mYFP and $AVR_{A13}$-1-mYFP) western blotting (WB) as indicated. CBB: Coomassie brilliant blue.

# Figure 3

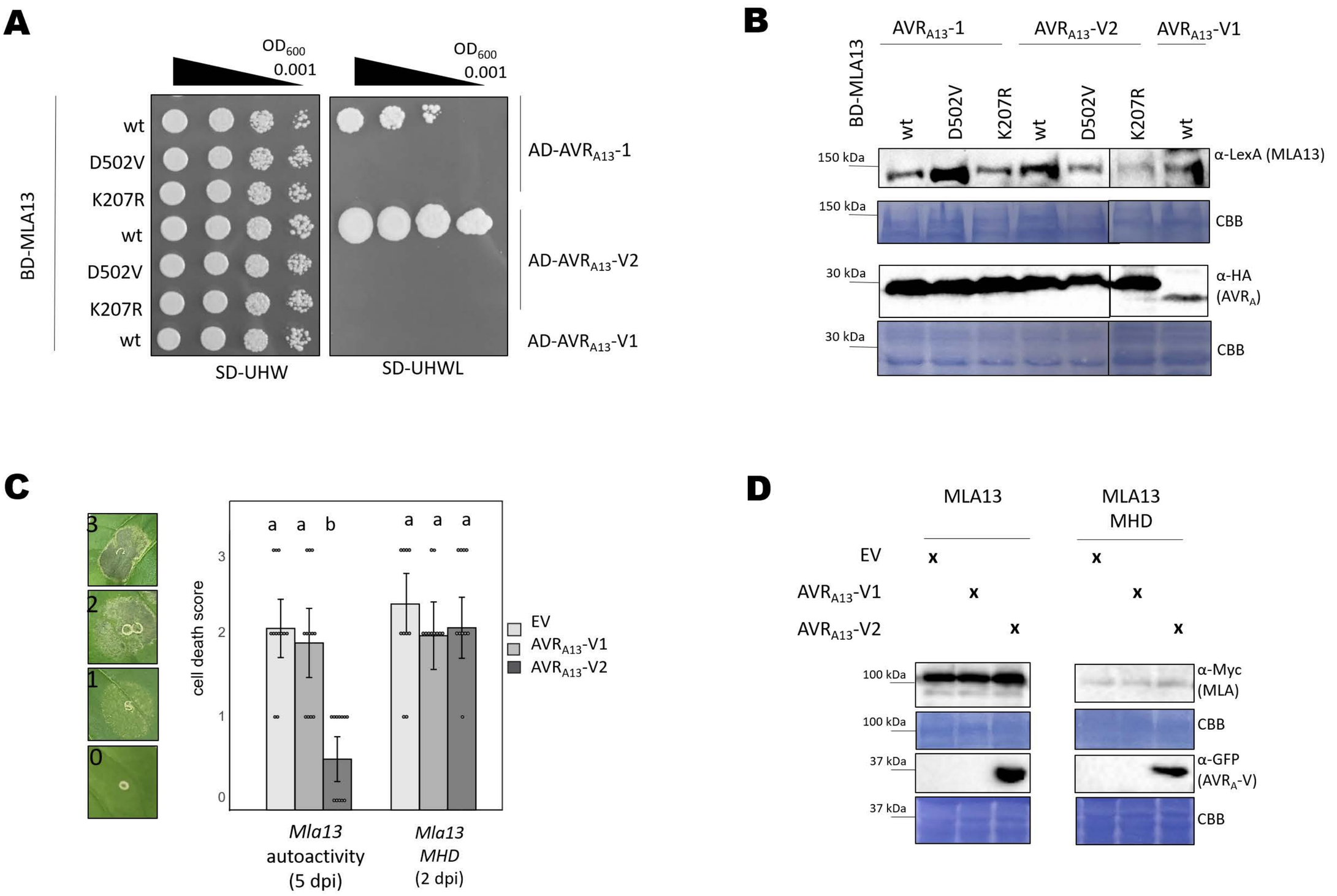




**Fig. 3: Amino acid exchanges in the nucleotide-binding site of MLA13 compromise $AVR_{A13}$ effector binding. (A, B)** Yeast cells were co-transformed with *Mla13 wt* or mutant variants *Mla13$^{D502V}$* (MHD) or *Mla13 K207R* (P-loop) fused N-terminally to the *LexA* binding domain sequence (BD) and *$AVR_{a13}$* variants lacking SPs fused N-terminally to the *B42* activation domain (AD) and *1xHA* tag sequence as indicated. **(A)** Growth of transformants was determined on selective growth media containing raffinose and galactose as carbon sources but lacking uracil, histidine and tryptophan (-UHW), and interaction of proteins was determined by leucine reporter activity reflected by growth of yeast on selective media containing raffinose and galactose as carbon sources, but lacking uracil, histidine, tryptophan and leucine (-UHWL). Figures shown are representatives of at least three experiments and pictures were taken 6 to 8 days after drop out. **(B)** Protein levels of BD-MLA13 variants and AD-$AVR_A$ variants corresponding to yeast of A. Yeast transformants were grown in raffinose and galactose containing selective media lacking uracil, tryptophan, and histidine to $OD_{600}$ = 1. Cells were harvested, total protein extracted, separated by gel electrophoresis, and western blots (WB) were probed with anti-LexA or anti-HA antibodies as indicated. **(C, D)** *Nicotiana benthamiana* leaves were co-transformed transiently with cDNAs of *$AVR_{a13}$-V1* or *$AVR_{a13}$*-V2 or *empty vector* (*EV*) together with constructs encoding either MLA13 or MLA13$^{D502V}$ (pAM-PAT vector) as indicated and under the control of the 35S promoter sequence at a 2:1 ratio. **(C)** Cell death was determined two (MLA13 MHD) to five days (MLA13) post transformation and scored from 0 to 3 based on the cell death scale indicated. All values obtained in at least three independent experiments are indicated by dots, error bars = standard deviation. Differences between samples were assessed by non-parametric Kruskal-Wallis and subsequent Dunn tests for each MLA variant. Calculated *P* values were as follows: MLA13: *p*=5E-05, MLA13 MHD*: p*=0.078. Samples marked by identical letters in the plots did not differ significantly ($p<0.05$) in the Tukey test for the corresponding MLA. **(D)** Protein levels corresponding to samples of C. Leaf tissue was harvested 36 hours post infiltration. Total protein was extracted, separated by gel electrophoresis and probed by anti-Myc (MLAs) or anti-GFP ($AVR_{A13}$-V2) western blotting (WB) as indicated. CBB: Coomassie brilliant blue.

# Figure 4

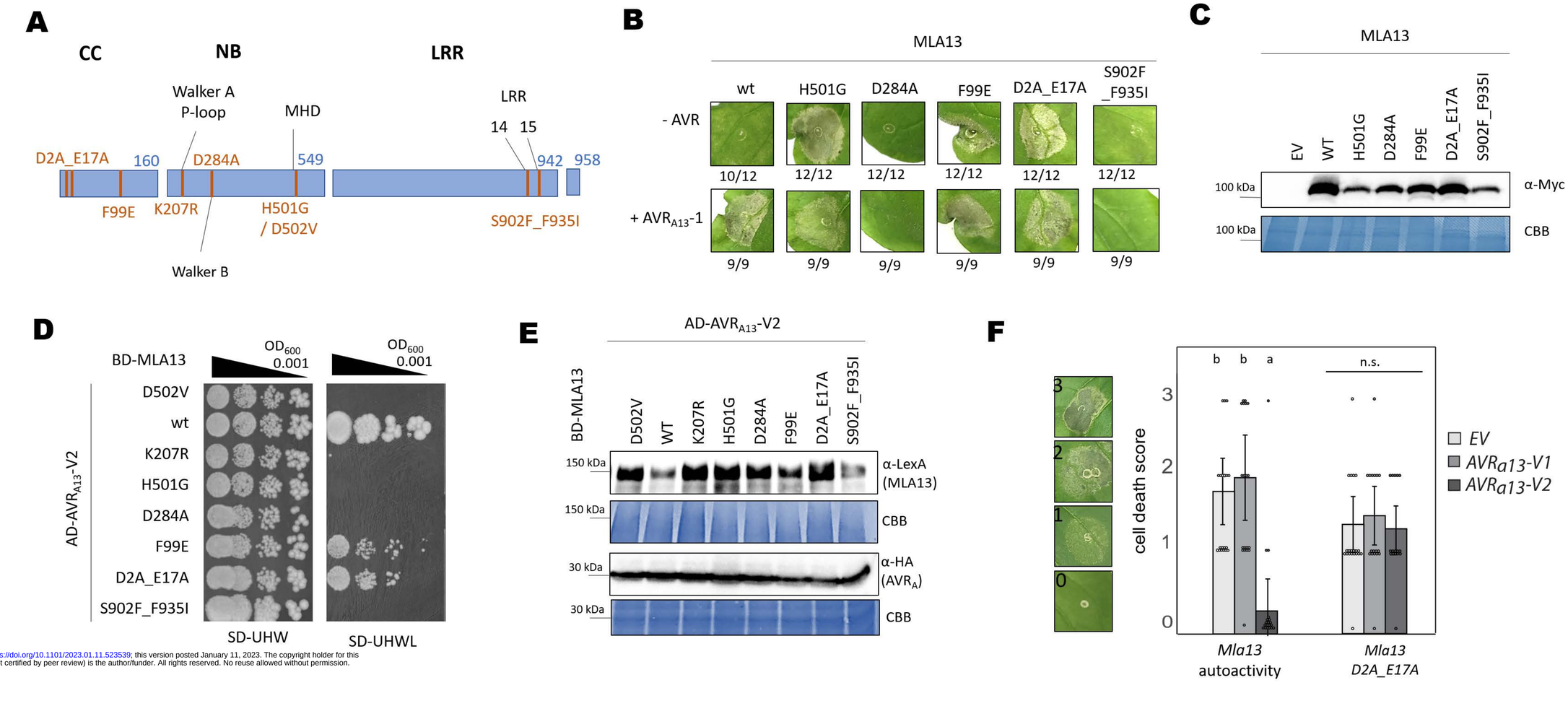




**Fig. 4: Amino acid (aa) exchanges in the coiled-coil (CC) domain de-regulate MLA13 auto-inhibition. (A)** Amino acid (aa) changes in MLA13 mutant variants. The D2A_E17A and the F99E variants encode changes in the MLA13 coiled-coil (CC) domain, which spans from aa1 to 160. The K207R, D284A, D502V and H501G variants encode changes in the nucleotide-binding site (NB, aa 161 to 549). The S902F_F935I variants affects the leucine-rich repeats (LRR, aa 550 to 942) which are followed by a short C-terminal amino acids sequence. **(B, C)** *Nicotiana benthamiana* leaves were transformed transiently with cDNAs of one of the *Mla13* variants as indicated (pGWB517 vector) either with or without $AVR_{a13}$*-1* lacking SPs and fused c-terminally to a *mYFP* sequence. All constructs are under the control of the 35S promotor. **(B)** Cell death was determined three days post transformation; n≥9. **(C)** Protein stability of the MLA variants fused to 4xMyc corresponding to constructs of B. Leaf tissue was harvested two days post infiltration. Total protein was extracted, separated by gel electrophoresis and probed by anti-Myc western blotting (WB) as indicated. **(D, E)** Yeast cells were co-transformed with *Mla13* variants fused N-terminally to the *LexA* binding domain (BD) sequence and $AVR_{a13}$-V2 lacking SPs fused N-terminally to the *B42* activation domain (AD) and *1xHA* tag sequence as indicated. Growth of transformants was determined on selective growth media containing raffinose and galactose as carbon sources but lacking uracil, histidine and tryptophan (-UHW), and interaction of proteins was determined by leucine reporter activity reflected by growth of yeast on selective media containing raffinose and galactose as carbon sources but lacking uracil, histidine, tryptophan and leucine (-UHWL). Figures shown are representatives of at least three experiments and pictures were taken 6 to 8 days after drop out. (**E**) Protein levels of BD-MLA13 variants and AD-$AVR_{A13}$-V2 corresponding to yeast of D. Yeast transformants were grown in raffinose and galactose containing selective media lacking uracil, tryptophan, and histidine to $OD_{600}$ = 1. Then, cells were harvested, total protein extracted, separated by gel electrophoresis, and western blots (WB) were probed with anti-LexA or anti-HA antibodies as indicated. CBB: Coomassie brilliant blue. **(F)** *N. benthamiana* leaves were co-transformed transiently with cDNAs of $AVR_{a13}$*-V1*, $AVR_{a13}$*-V2* or *empty vector* (*EV*) together with constructs encoding the MLA13 variant as indicated and under the control of the 35S promoter sequence at a 2:1 ratio. Cell death was determined three days post transformation and scored from 0 to 3 based on the cell death scale indicated. All values obtained in at least two independent experiments are indicated by dots, error bars = standard deviation. Differences between samples were assessed by non-parametric Kruskal-Wallis and subsequent Dunn tests for each MLA variant. Calculated *P* values were as follows: MLA13*: p* = 9.38E-07, $MLA13^{D2A\_E17A}$: *p* = 0.77. n.s. = no significant difference.

# Figure 5



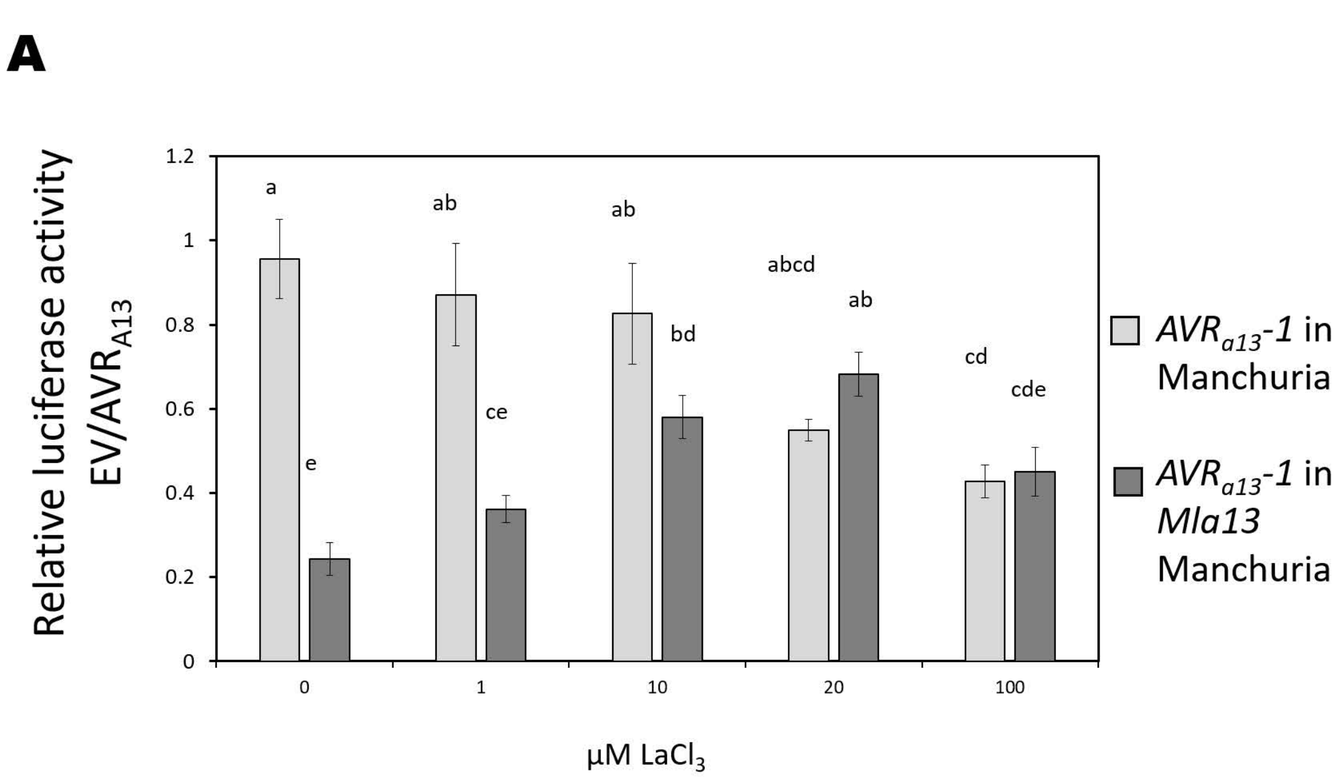


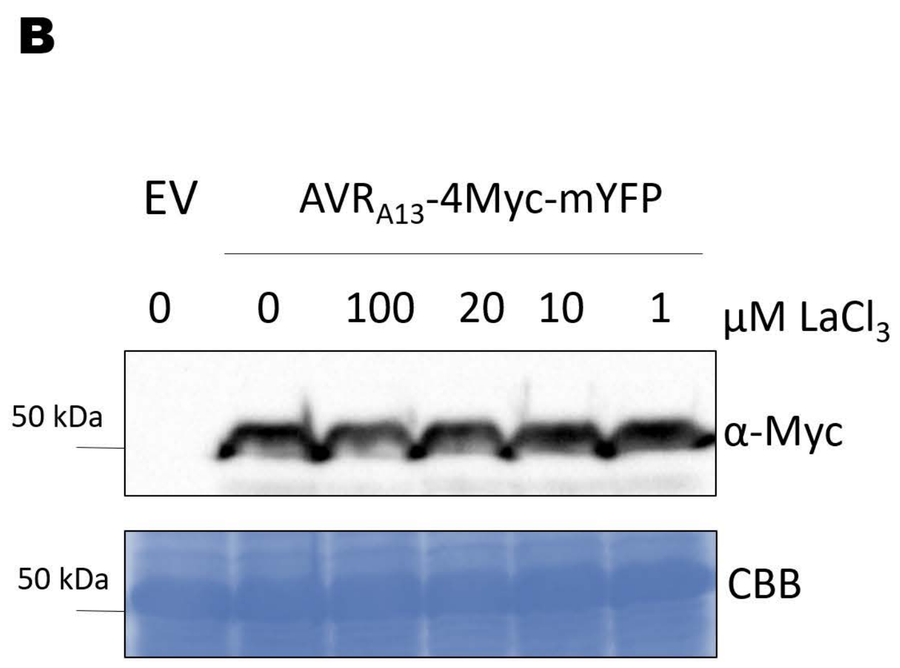


**Fig. 5: Calcium channel activity is required for *Mla13*-mediated cell death in barley (A)** Barley protoplasts of lines CI 16155 (cultivar Manchuria *Mla13*) and CI2330 (Manchuria) were transfected with *pUBQ:luciferase* and piPKb002 containing *AVR$_{a13}$-1* cDNA without signal peptide or a piPKb002 empty vector control and recovered in the presence of $LaCl_3$ at concentrations indicated. Luciferase activity was determined 16 hr post transfection/addition of $LaCl_3$ as a proxy for cell death and normalized against the respective *EV* sample. Error bars = standard deviation. Differences between samples were assessed using non-parametric Kruskal-Wallis and subsequent Dunn's post hoc tests. *p*= 6.179e-10. Samples marked by identical letters in the plot did not differ significantly ($p<0.05$) in Dunn's test. **(B)** Protoplasts derived from cultivar Manchuria CI2330 leaves transfected with *pZmUBQ:AVR$_{a13}$-1-mYFP* were harvested 16h post transfection/$LaCl_3$ treatment. Total protein was extracted, separated by gel electrophoresis, and western blots (WB) were probed with anti-GFP antibodies. CBB: Coomassie brilliant blue.

# Figure S1



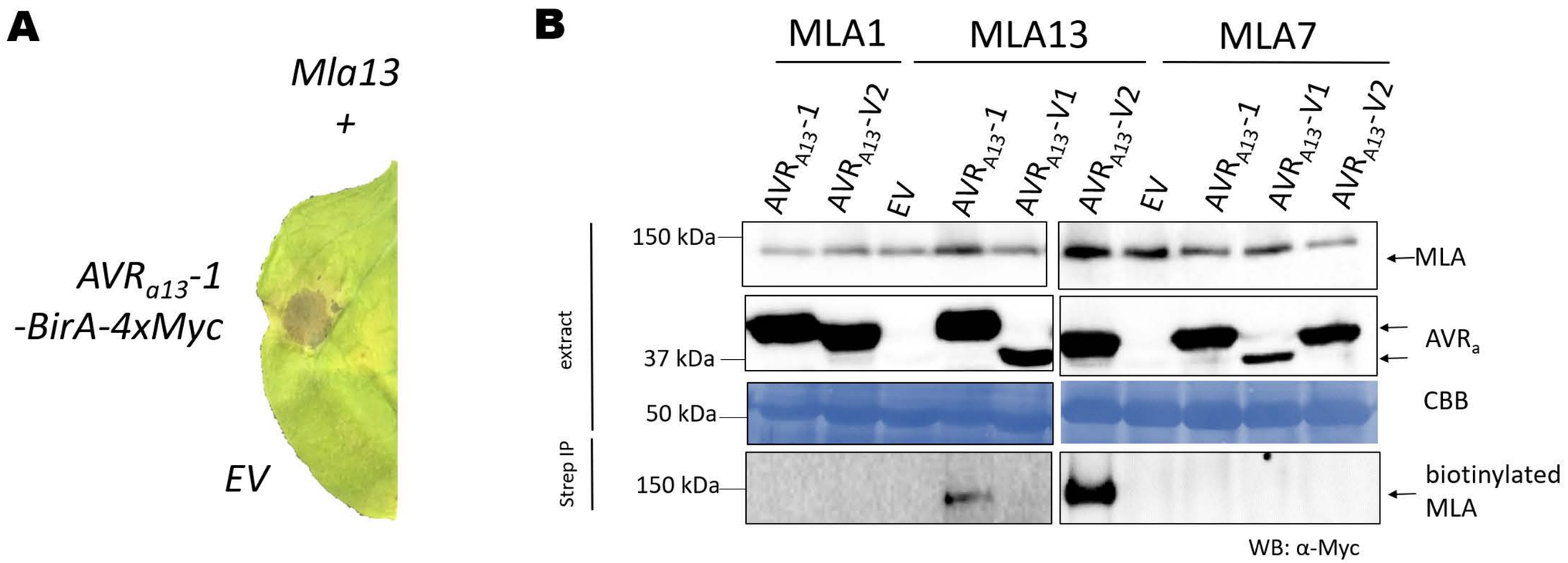


**Figure S1: (A)** *Nicotiana benthamiana* leaves were transformed transiently with cDNAs of the *Mla13* together with *empty vector* (*EV*) or *AVR$_{a13}$-1* lacking SPs and fused c-terminally to *BirA-4Myc* tag sequence and expressed from the 35S promotor. Cell death was determined three days post transformation and picture shows representative of at least three independent leaves. **(B)** *N. benthamiana* leaves were transformed transiently with cDNAs of *Mla1* or *Mla7* or *MLA13* fused C-terminally to a *4xMyc* sequence and at 24 h before re-transformation with cDNAs encoding *AVR$_{a13}$-1-BirA-4xMyc, AVR$_{a13}$-V1-BirA-4xMyc, AVR$_{a13}$-V2-BirA-4xMyc* or *empty vector* (*EV*) as indicated. All leaves were treated with 10 µM biotin by infiltration at 24h after the second transformation. Leaf tissue was harvested 24h post biotin treatment. Total protein was extracted under denaturing conditions and recovered by Strep IP, separated by gel electrophoresis and probed by anti-Myc western blotting (WB). CBB: Coomassie brilliant blue.

# Figure S2



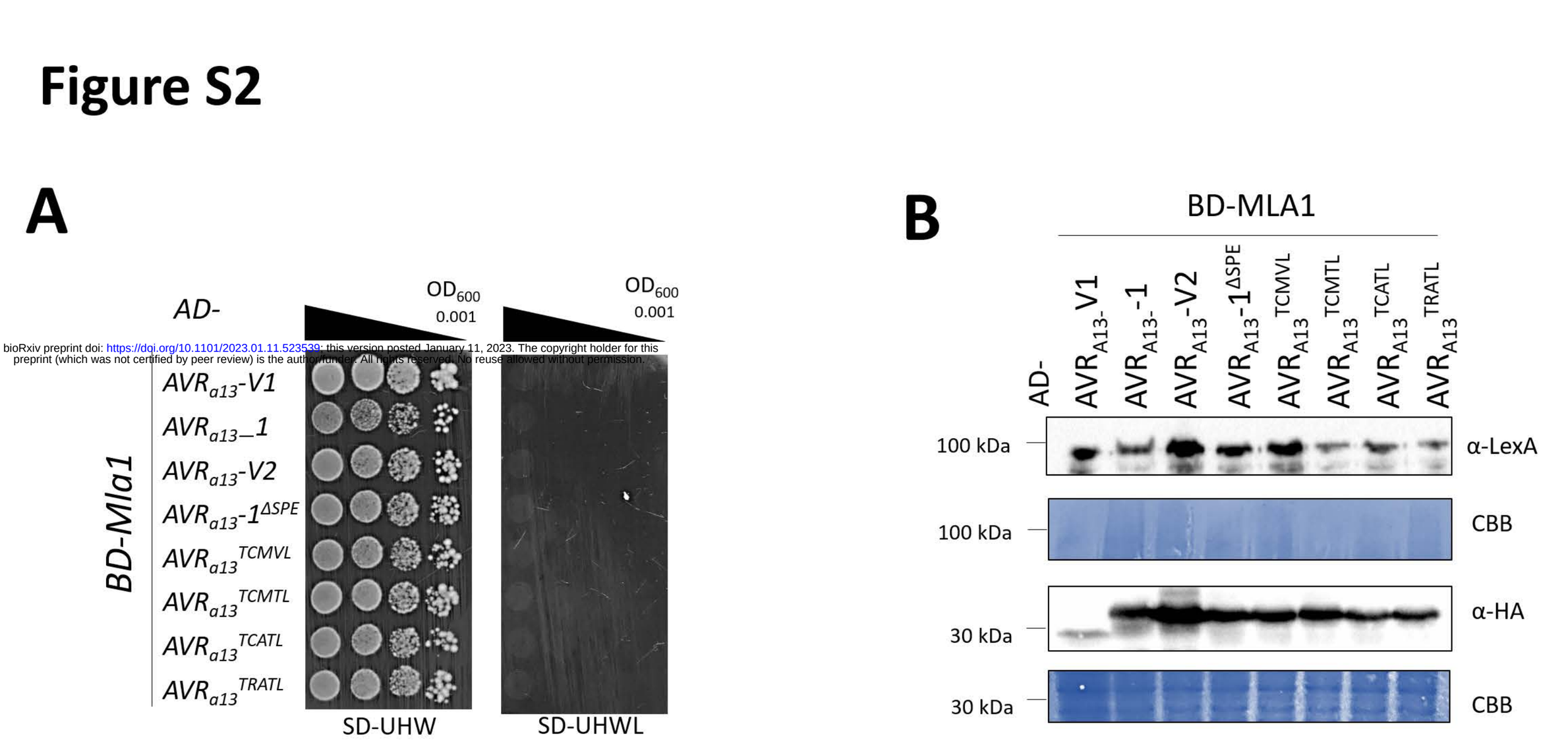


**Fig. S2: Specificity control to Figure 1D. (A,B)** Yeast cells were co-transformed with *Mla1* fused N-terminally to the *LexA* binding domain sequence (BD) and $AVR_{a13}$ variants lacking SPs fused N-terminally to the *B42* activation domain (AD) and 1xHA tag sequence as indicated. Growth of transformants was determined on selective growth media containing raffinose and galactose as carbon sources but lacking uracil, histidine and tryptophan (-UHW), and interaction of proteins was determined by leucine reporter activity reflected by growth of yeast on selective media containing raffinose and galactose as carbon sources but lacking uracil, histidine, tryptophan and leucine (-UHWL). Figures shown are representatives of at least three experiments and pictures were taken 6 to 8 days after drop out. (B) Protein levels of BD-MLA1 and AD-$AVR_A$ variants corresponding to yeast of D. Yeast transformants were grown in raffinose and galactose containing selective media lacking uracil, tryptophan, and histidine to $OD_{600}$ = 1. Then, cells were harvested, total protein extracted, separated by gel electrophoresis, and western blots (WB) were probed with anti-LexA or anti-HA antibodies as indicated. CBB: Coomassie brilliant blue.

# Figure S3

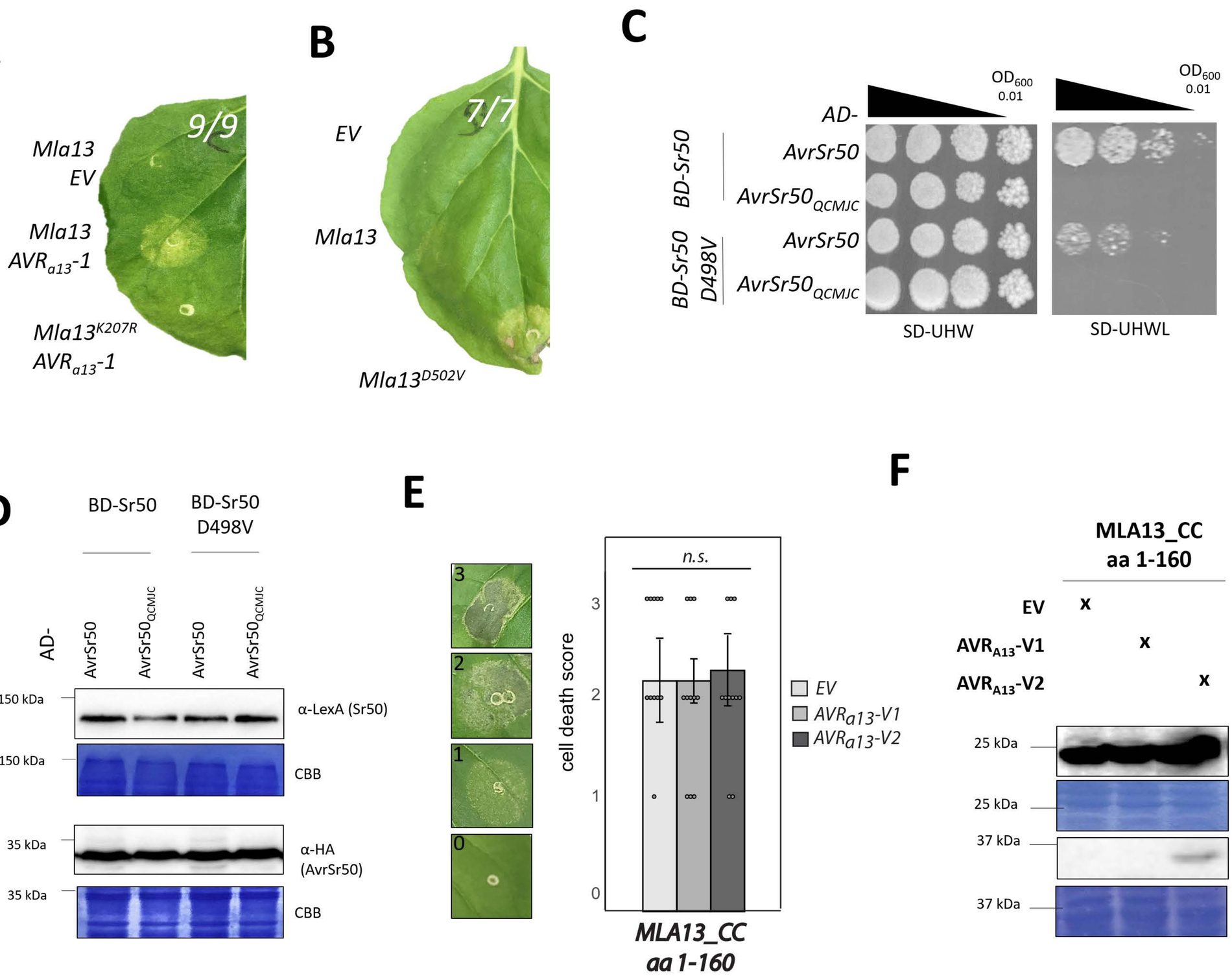


**Fig. S3: (A, B)** *Nicotiana benthamiana* leaves were co-transformed transiently with *empty vector* (*EV)* or constructs encoding either MLA13, MLA13 K207D or MLA13 D502V (pGWB) as indicated with (A) or without (B) cDNA encoding of *AVR$_{a13}$-1* or *EV.* All cDNAs were under the control of the 35S promoter sequence. Cell death was determined three days post transformation. **(C, D)** Yeast cells were co-transformed with Sr50 or Sr50 D498V fused N-terminally to the *LexA* binding domain sequence (BD) and AvrSr50 variants lacking SPs fused N-terminally to the *B42* activation domain (AD) and 1xHA tag sequence as indicated. Growth of transformants was determined on selective growth media containing raffinose and galactose as carbon sources but lacking uracil, histidine and tryptophan (-UHW), and interaction of proteins was determined by leucine reporter activity reflected by growth of yeast on selective media containing raffinose and galactose as carbon sources but lacking uracil, histidine, tryptophan and leucine (-UHWL). Figures shown are representatives of at least three experiments and pictures were taken 12 to 14 days after drop out. (B) Protein levels of BD-Sr50 and AD-AvrSr50 variants corresponding to yeast of C. Yeast transformants were grown in raffinose and galactose containing selective media lacking uracil, tryptophan, and histidine to $OD_{600}$ = 1. Then, cells were harvested, total protein extracted, separated by gel electrophoresis, and western blots (WB) were probed with anti-LexA or anti-HA antibodies as indicated. **(E)** *Nicotiana benthamiana* leaves were co-transformed transiently with cDNAs of *AVR$_{a13}$-V1* or *AVR$_{a13}$*-V2 or *empty vector* (*EV*) together with constructs encoding the MLA13 coiled-coil (CC) domain (aa 1-160). **(E)** Cell death was determined two days post transformation and scored from 0 to 3 based on the cell death scale indicated. All values obtained in at least three independent experiments are indicated by dots, error bars = standard error. Differences between samples were assessed by the non-parametric Kruskal-Wallis test. *p*= 0.623871; n.s. = not significant. **(F)** Protein levels corresponding to samples of C. Leaf tissue was harvested 36 hours post infiltration. Total protein was extracted, separated by gel electrophoresis and probed by anti-Myc (MLA13_CC) or anti-GFP ($AVR_{A13}$-V2) western blotting as indicated. CBB: Coomassie brilliant blue.

# Figure S4

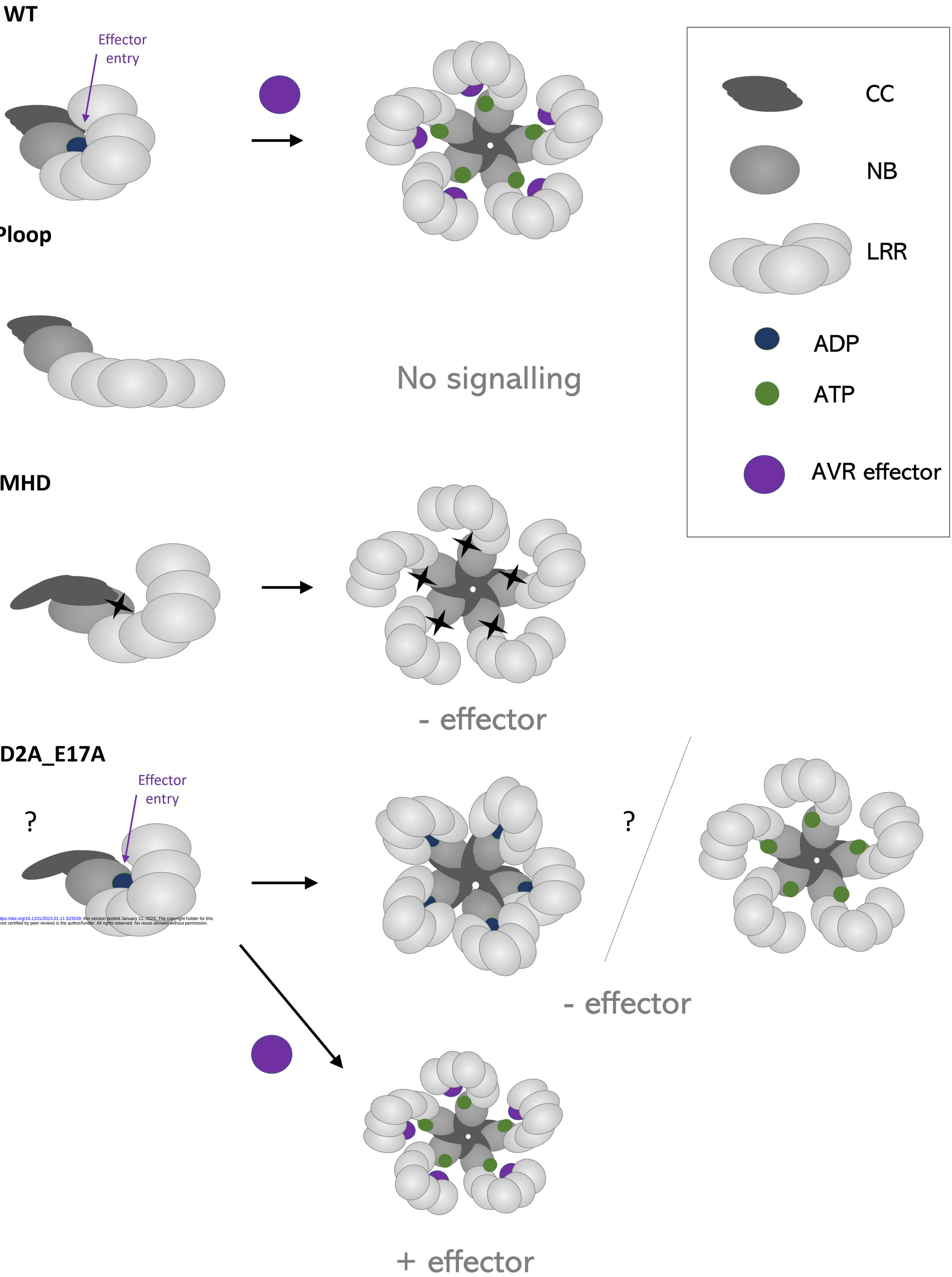




**Fig. S4:** Schematic models of monomeric and oligomeric MLA13 wild type, MLA13 P-loop, MLA13 MHD and MLA13$^{D2A_E17A}$ conformations with indication of putative effector (purple) entry sites and binding of ADP (green) or ATP (blue).

# Figure S5

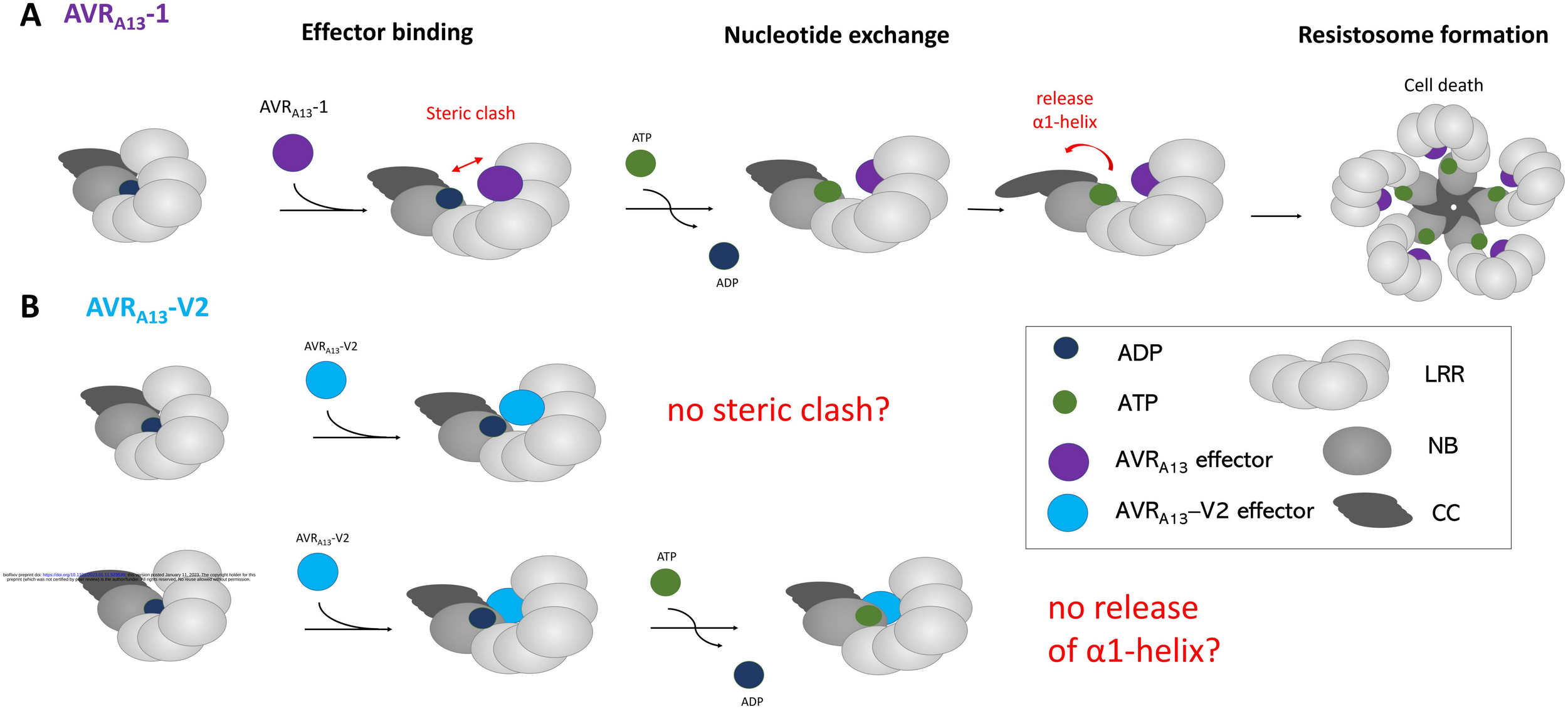




**Fig. S5:** Schematic models of MLA13 during the multistep process of putative resistosome formation initiated by the interaction with *Bgh* AVR$_{A13}$-1 (A) and putative models for the inhibition of the activation process by AVR$_{A13}$-V2 (B). (**A**) AVR$_{A13}$-1 binding to the effector entry point involving the MLA13 Leucine-rich-repeats (LRR) domain leads to a steric clash and subsequent replacement of adenosine diphosphate (ADP) by adenosine triphosphate ATP) in the nucleotide-binding (NB) pocket of the MLA13. ATP-binding causes additional structural rearrangement of the N-terminal Coiled-coil (CC) domain releasing the α1-helix. In the resulting putative pentameric wheel-like MLA13 resistosome, the α1-helices are thought to form a funnel like structure. (**B**) AVR$_{A13}$-V2 binding is likely either incapable to inducing a steric clash or prevents subsequent release of the α1-helix.